

2012

Electric elevator drive with position control

Peter James Ford

Louisiana State University and Agricultural and Mechanical College, peter.ford.ee@gmail.com

Follow this and additional works at: https://digitalcommons.lsu.edu/gradschool_theses



Part of the [Electrical and Computer Engineering Commons](#)

Recommended Citation

Ford, Peter James, "Electric elevator drive with position control" (2012). *LSU Master's Theses*. 2938.
https://digitalcommons.lsu.edu/gradschool_theses/2938

This Thesis is brought to you for free and open access by the Graduate School at LSU Digital Commons. It has been accepted for inclusion in LSU Master's Theses by an authorized graduate school editor of LSU Digital Commons. For more information, please contact gradetd@lsu.edu.

ELECTRIC ELEVATOR DRIVE WITH POSITION CONTROL

A Thesis
Submitted to the Graduate Faculty of the
Louisiana State University and
Agricultural and Mechanical College
in partial fulfillment of the
requirements for the degree of
Master of Science

in

Electrical Engineering

by
Peter James Ford
B.S., Louisiana State University Agricultural and Mechanical College, 2009
May 2012

Dedicated to my parents

Acknowledgements

I would like to thank those who have provided me the opportunity to write this thesis: My parents who have always provided the motivation and support I needed to pursue an education in Electrical Engineering. My advisor and mentor Dr. Ernest A. Mendrela, who has been a guiding light along my path to both my Bachelor's and my Master's degree in Electrical Engineering. Finally, I would like to thank the faculty and staff of Louisiana State University's Department of Electrical and Computer engineering: Dr. Kemin Zhou, Dr. Alex Skavantos, and Dr. Shahab Mehraeen who took the time and care to serve on my defense committee and Mrs. Beth Cochran, the graduate program coordinator, has worked tirelessly to ensure my interest in the department were looked after.

Table of Contents

Dedication.....	ii
Acknowledgements.....	iii
List of Tables.....	vi
List of Figures.....	vii
Abstract.....	x
Chapter 1: Introduction.....	1
1.1 Permanent-Magnet DC Motors.....	1
1.2 Digital Control Systems.....	1
1.3 Elevators.....	2
1.4 Teaching Lab.....	2
1.5 Objectives of Thesis.....	2
1.6 Brief Description of Chapters.....	3
Chapter 2: Electric Elevator Drive.....	4
2.1 Commercial Electric Elevator Drive Systems.....	4
2.1.1 Kone System.....	4
2.1.2 Otis System.....	6
2.2 Laboratory Model of an Elevator with Permanent-Magnet DC Drive.....	7
2.3 Mathematical Model of Elevator Electric Drive.....	8
2.3.1 Motor's Electrical Equations.....	8
2.3.2 Mechanical System's Motion Equations.....	9
Chapter 3: Determination of Parameters of Electric Elevator Drive.....	13
3.1 Steady-State Parameters.....	13
3.2 Dynamic Parameters.....	21
Chapter 4: Designing of Control System.....	28
4.1 Feedback Control of Electric Drive.....	28
4.2 Current Control Loop.....	31
4.3 Speed Control Loop.....	35
4.4 Position Control Loop.....	38
Chapter 5: Performance of Electric Elevator Drive with Position Control.....	40
5.1 Performance of Simulated Electric Elevator Drive with Position Control.....	40
5.2 Performance of Experimental Electric Elevator Drive with Position Control.....	54
5.3 Comments on Performance of Electric Elevator Drive with Position Control.....	66

Chapter 6: Conclusions.....	67
References.....	69
Appendix A: Load_Simulation_Parameters.....	70
Appendix B: Plot_Simulation.....	71
Appendix C: Plot_RealTime.....	72
Vita.....	73

List of Tables

Table 3.1	Steady-state parameter determination data.....	16
Table 3.2	Linearized data received from ω_m versus I_a characteristics.....	18
Table 3.3	Average values of motor parameters obtained from steady-state characteristics.....	19
Table 3.4	Steady-state friction determination data.....	20
Table 3.5	Steady-state friction parameters.....	21
Table 3.6	Inductance of armature winding.....	24
Table 3.7	Results of equivalent inertia J_{eq} calculations.....	26
Table 3.8	Data for determination of equivalent inertia J_{eq}	27
Table 4.1	Parameters for current control loop design.....	35
Table 4.2	Torque control loop integral gain calculations.....	35
Table 4.3	Parameters for speed control loop design.....	37
Table 4.4	Results of speed loop gain calculations.....	37
Table 4.5	Position loop proportional gain calculations.....	39
Table 5.1	Simulated position response of electric elevator drive with no load and 1kg, 2kg load.....	53
Table 5.2	Percent change in simulated position response of electric elevator drive under load.....	53
Table 5.3	Real-time position response of elevator electric drive with no load and 1kg, 2kg load.....	65
Table 5.4	Percent change in real-time position response of electric elevator drive under load.....	66
Table 5.5	Performance of Elevator Electric Drive.....	66

List of Figures

Figure 2.1 Kone EcoDisc© electric elevator drive[4]	5
Figure 2.2 Kone Machine-Room-Less Elevator System [3,4]	5
Figure 2.3 Otis steel belt [7]	6
Figure 2.4 OtisGen2© electric elevator drive [7].....	6
Figure 2.5 Laboratory model of elevator driven by permanent-magnet DC motor.....	7
Figure 2.6 Equivalent circuit of armature of DC motor.....	8
Figure 3.1 $\omega_m = f(I_a)$ Characteristic 14.....	14
Figure 3.2 MUT connected to load motor.....	14
Figure 3.3 MUT axially coupled to load motor (seen in laboratory).....	15
Figure 3.4 Speed versus armature current characteristics.....	18
Figure 3.5 Torque-speed characteristic of steady-state friction model.....	21
Figure 3.6 Current response with blocked rotor ($\omega_m = 0$).....	22
Figure 3.7 Current waveform for 3V step increase.....	23
Figure 3.8 System speed response upon shutdown.....	25
Figure 3.9 Speed response after power supply is disconnected from motors.....	26
Figure 4.1 Feedback control system of DC motor.....	28
Figure 4.2 Cascaded control system.....	29
Figure 4.3 PI Controller Diagram.....	30
Figure 4.4 Expanded current control loop[6]	31
Figure 4.5 Reduced current control loop[6]	32
Figure 4.6 Simplified current control loop[6]	32

Figure 4.7 Simplified current control loop[6]	36
Figure 4.8 Position control loop block diagram.....	38
Figure 5.1 Simulink model of elevator electric drive with position control.....	41
Figure 5.2 Simulated DC machine subsystem.....	41
Figure 5.3 Simulated current controller subsystem.....	42
Figure 5.4 Simulated speed controller subsystem.....	43
Figure 5.5 Simulated position controller subsystem.....	43
Figure 5.6 Simulated load torque subsystem for ascending elevator car.....	44
Figure 5.7 Simulated load torque subsystem for descending elevator car.....	44
Figure 5.8 Simulated reference position of elevator electric drive with ascending car.....	45
Figure 5.9 Simulated reference position of elevator electric drive with descending car.....	45
Figure 5.10 Simulated position response of elevator electric drive with ascending car.....	46
Figure 5.11 Simulated position response of elevator electric drive with descending car.....	46
Figure 5.12 Simulated speed response of elevator electric drive with ascending car.....	47
Figure 5.13 Simulated speed response of elevator electric drive with descending car.....	47
Figure 5.14 Simulated current response of elevator electric drive with ascending car.....	48
Figure 5.15 Simulated current response of elevator electric drive with descending car.....	48
Figure 5.16 Simulated torque response of elevator electric drive with ascending car.....	49
Figure 5.17 Simulated torque response of elevator electric drive with descending car.....	49
Figure 5.18 Simulated voltage response of elevator electric drive with ascending car.....	50
Figure 5.19 Simulated voltage response of elevator electric drive with descending car.....	50
Figure 5.20 Simulated position response of elevator electric drive for ascending car carrying no load, 1kg load, and 2kg load.....	52

Figure 5.21 Simulated position response of elevator electric drive for descending car carrying no load, 1kg load, and 2kg load.....	52
Figure 5.22 View of experimental elevator in lab.....	54
Figure 5.23 Safety cut-off switch.....	55
Figure 5.24 View of elevator electric drive and drive pulley with drive belt.....	55
Figure 5.25 Elevator electric drive's power processing unit.....	56
Figure 5.26 dSpace 1104 hardware.....	56
Figure 5.27 Real-time Simulink model for position control of elevator electric drive.....	57
Figure 5.28 Real-time current controller subsystem.....	58
Figure 5.29 Real-time speed controller subsystem.....	58
Figure 5.30 Real-time position controller subsystem.....	59
Figure 5.31 Real-time duty cycle generation subsystem.....	59
Figure 5.32 Real-time speed averaging subsystem.....	59
Figure 5.33 Control desk control interface for position control of elevator's electric drive.....	60
Figure 5.34 Real-time position response of elevator electric drive with ascending car.....	61
Figure 5.35 Real-time position response of elevator electric drive with descending car.....	61
Figure 5.36 Real-time speed response of elevator electric drive with ascending car.....	62
Figure 5.37 Real-time speed response of elevator electric drive with descending car.....	62
Figure 5.38 Real-time current response of elevator electric drive with ascending car.....	63
Figure 5.39 Real-time current response of elevator electric drive with descending car.....	63
Figure 5.40 Real-time position response of elevator electric drive for ascending car carrying no load, 1kg load, and 2kg load.....	64
Figure 5.41 Real-time position response of elevator electric drive for descending car carrying no load, 1kg load, and 2kg load.....	65

Abstract

This thesis is a study on the implementation of an elevator's position-controlled electric drive. The information contained within this paper serves as a framework to expand the usefulness of electric drives through the addition of digital control systems and switching power supplies. The tangible example of an elevator driven by a permanent-magnet DC motor is used for this paper so that students may relate to the work and apply it to their future projects. The tasks to be accomplished in order to achieve an electric elevator drive with position control are: determining the parameters of the permanent-magnet DC motor, designing a control system to direct the motor as desired, and verifying the performance of the system through use of computer simulations and experimental testing. The tests to derive the motor parameters as well as the theory behind the test are covered in depth before the design procedures for creating a cascaded control system are started. Computer simulations are conducted using the parameters and controllers which will be implemented in real-time before experimental testing in the lab begins. Conclusions are drawn about the performance of the position-controlled electric elevator drive based upon the simulation and experimental results. The implementation of an elevator driven by a permanent-magnet DC motor with position control is successful and provides an illustrative example to those who wish to apply electric drives to various mechanical systems.

Chapter 1: Introduction

This thesis will cover the design, simulation, and implementation of a permanent-magnet DC motor controlled by a digital control system to drive a suspension-system elevator in such a way that the material in this thesis can be used as a teaching tool and laboratory experiment for the LSU Course EE 4490 Advanced Speed Drives.

1.1 Permanent-Magnet DC Motors

The permanent-magnet DC motor is an ideal choice for driving mechanical systems where precise speed control is desired. Regulating the speed of a permanent-magnet DC motor is as simple as changing the magnitude of voltage applied to the motor's armature circuit; to make the motor operate in the opposite direction the polarity of the supply voltage needs to only be reversed. A switching power supply and digital control system provided an efficient means for doing this.

1.2 Digital Control Systems

Digital control systems are composed of software and hardware components which are optimized to execute algorithms quickly and efficiently. These algorithms are designed to speed up complex operations which may involve mathematical calculations and logic operations as well as the conversion of analog signals into a digital format or digital signals into an analog format. These algorithms can be executed as optimized code on a microprocessor or they can be hardwired into the controller's architecture. In order to increase efficiency and obtain the quickest response time each digital control system is designed for the system it must regulate. Using a digital control system to dictate the position, speed, and current of an elevator's electric drive increases the accuracy and precision with which the elevator system responds to position commands.

1.3 Elevators

Elevators are used to move loads from one height to another without disturbing the load itself. The prime mover of an elevator can either be a hydraulic tube beneath the elevator cart which rises as fluid is pumped in to or out of the cylinder or an elevator can be moved using a cable system and counterweight which is driven by an electric motor [8]. Suspension systems driven by electric motors are the ideal choice for applications having minimal space and great heights because these systems do not require infrastructure to be built beneath the floor of the elevator and are limited in height only by the ability of the electric drive to overcome static forces such as gravity and dynamic forces such as friction and air drag. For these reasons this thesis will focus on the suspension system driven by an electric motor.

1.4 Teaching Lab

This thesis is to be an example of implementing position, speed, and current control of a permanent-magnet DC motor to drive a mechanical system which can be used as a teaching tool in the LSU electrical engineering course on electric drives. Students will be able to apply the lessons and techniques contained within this paper to other applications of digitally controlled electric machines beyond the position controlled electric elevator drive.

1.5 Objectives of the Thesis

- To implement position control of an elevator's permanent-magnet DC motor drive
- To develop the experiment on position control of a permanent-magnet DC motor drive as teaching lab for the LSU electrical engineering course on electric machines

1.6 Brief Description of Chapters

- Chapter 2 is a review of electrically driven elevators and will cover two designs currently being used in commercial applications in addition to covering the elevator model to be used in this thesis
- Chapter 3 concerns the determination of parameters for the elevator's electric drive
- Chapter 4 covers the design of the digital control system which dictates the elevator's electric drive's response to position input
- Chapter 5 summarizes the performance of the elevator's electric drive, both in computer simulation and experimental implementation.
- Chapter 6 gives conclusions based upon the analysis contained within the thesis and elaborates upon its potential use for education

Chapter 2: Electric Elevator Drive

The physical arrangement of a suspension-type elevator has a direct affect on the forces acting upon its propulsion system. Ideally, a gear system is not used so as to reduce mechanical losses and improve the drive system's response time; however, a drive system without gears requires a motor capable of accelerating the system from a standstill. To aid the drive system, a counterweight is employed to reduce the overall force needed to drive the system when it is under load. To further reduce the work which must be done by the prime mover, the support cable/belt is configured to spread the load evenly between the drive pulley and the anchor points. These techniques of reducing the load force on the drive system are applied to all commercial elevators of the suspension type regardless of their propulsion system leaving the electric drive to be the defining factor of each company's design.

2.1 Commercial Electric Elevator Drive Systems

Two major international manufactures of elevators using electric drives are Kone and Otis. Both companies use the same approach to suspension of car and counterweight but have developed different electric drive systems for propelling the elevator car and counterweight.

2.1.1 Kone System

The Kone EcoDisc© elevator electric drive system is a machine-room-less design which places a permanent-magnet, synchronous motor in the hub of the drive pulley as seen in Fig. 2.1. Steel cables are passed over this drive pulley and suspended the car and counterweight; as shown in Fig. 2.2, these cables are anchored to the top of the elevator shaft and cable tension is provided by the weight of the hanging car and counter-weight. In this arrangement when the elevator car moves upwards the counterweight moves downwards with cable ends never changing position.



Figure 2.1 Kone EcoDisc© electric elevator drive [4]

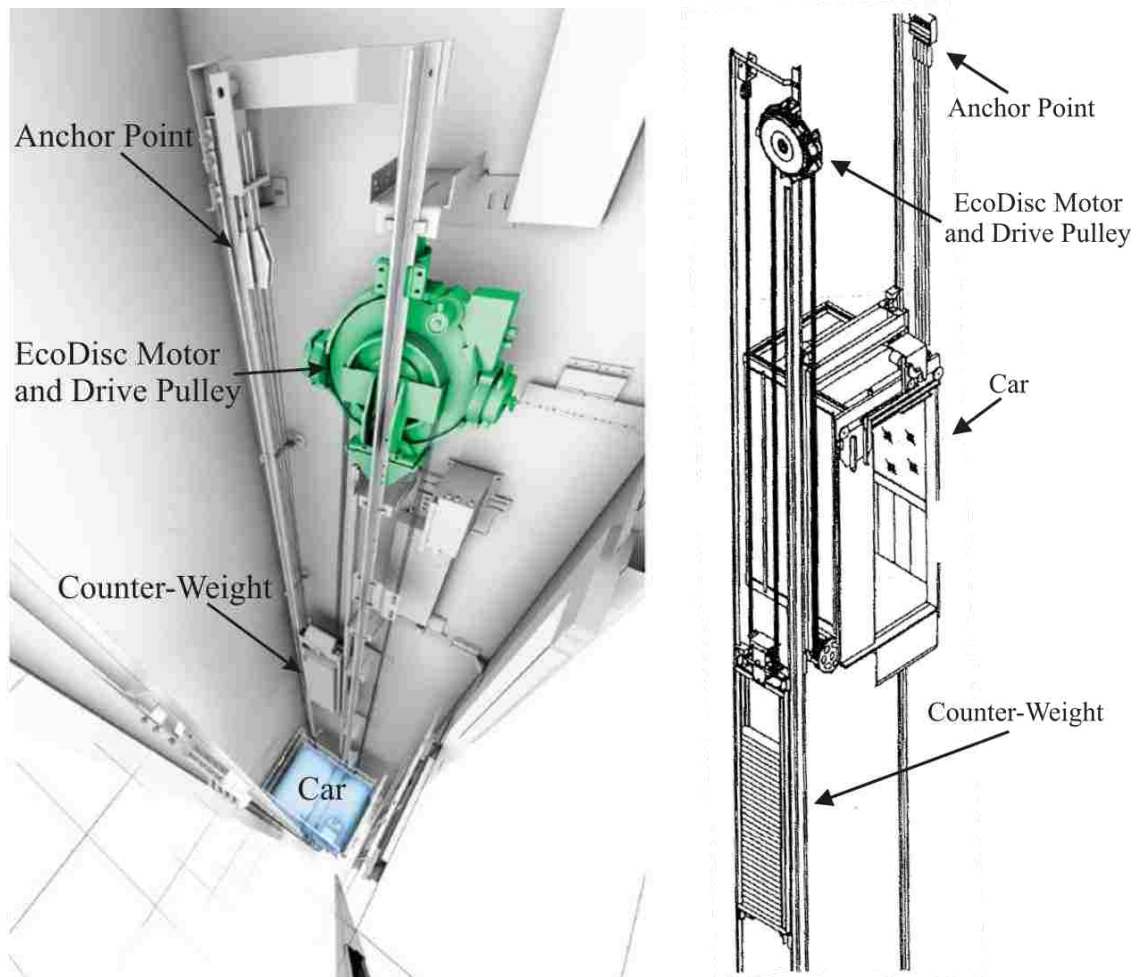


Figure 2.2 Kone Machine-Room-Less Elevator System [3,4]

2.1.2 Otis System

The OtisGen2© electric elevator drive system is a machine-room-less design which uses a flat steel belt (see Fig. 2.3) in place of woven steel cables to support the elevator car and counter weight [7]. The use of a belt allows for a drive pulley with a smaller diameter which reduces the total volume of the drive system (see Fig. 2.4). This smaller drive system is mounted at the top of the elevator shaft which eliminates the need for an equipment room to be built above the elevator shaft, hence the moniker “machine-room-less”. Like the Kone system, the OtisGen2© electric elevator drive system is powered by a permanent-magnet synchronous motor. Also like the Kone system, the Otis system has the elevator car and counterweight suspended from the drive pulley with the ends of the belt anchored to the top of the elevator shaft so that the suspended car and counterweight provide tension on the belt.



Figure 2.3 Otis steel belt [7]



Figure 2.4 OtisGen2© electric elevator drive [7]

2.2 Laboratory Model of an Elevator with Permanent-Magnet DC Drive

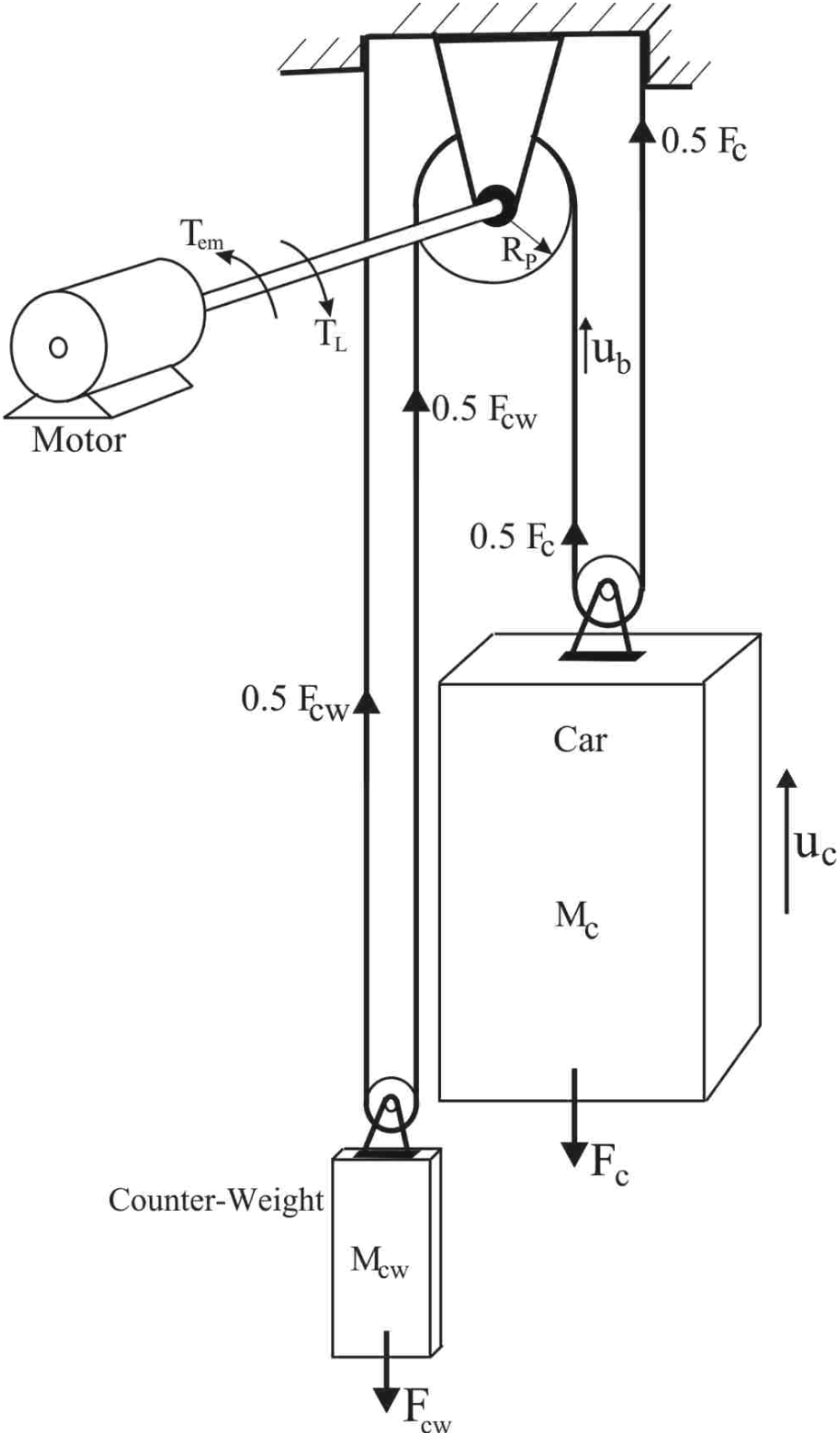


Figure 2.5 Laboratory model of elevator driven by permanent-magnet DC motor

The elevator electric drive that is proposed for this thesis is most similar to the Otis methodology. The scheme of proposed structure is shown in Fig. 2.5. A drive belt is looped over a drive pulley with the ends anchored to the top of the elevator shaft. The electric drive is rigidly attached to the drive pulley without the use of gearing. The car and counterweight, which ride on pulleys, provide belt tension ensuring the toothed belt and drive pulley do not slip. The elevator car and counter-weight are of equal weight so as to reduce load on the motor to only what is placed inside the cart.

2.3 Mathematical Model of Elevator Electric Drive

The equations governing the operation of the elevator can be attributed to the motor's electrical circuit and to its mechanical system.

2.3.1 Motor's Electrical Equations

The elevator is driven by a permanent-magnet DC motor. The equivalent circuit of the permanent-magnet DC motor is confined to the armature circuit which is illustrated in Fig. 2.6.

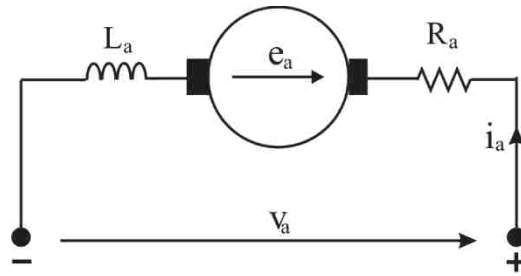


Figure 2.6 Equivalent circuit of armature of DC motor

The motor voltage equation of the armature circuit is:

$$V_a = e_a + R_a \cdot i_a + L_a \frac{di_a}{dt} \quad (2.1)$$

where:

$$e_a = K \cdot \omega_m \text{ is the electro-motive force developed in the armature's winding} \quad (2.2)$$

K is the motor constant

ω_m is the angular speed of the motor's shaft

V_a is the voltage difference between the armature terminals

R_a is the resistance of the armature circuit

i_a is the current flowing through the armature circuit

L_a is the inductance of the armature circuit

The electro-magnetic torque T_{em} developed by the motor is expressed as:

$$T_{em} = K \cdot i_a \quad (2.3)$$

2.3.2 Mechanical System's Motion Equations

In order to derive the motion equation that describes the elevator's mechanical system it is assumed that the mass of the drive belt is ignored due to its material composition and length. In practice, the drive belt or drive cable is constructed from steel and its significant mass contributes to the load torque in a non-linear fashion depending upon the position of the car.

The motion equation of the entire system from the motor's perspective is:

$$T_{em} = J_M \frac{d\omega_m}{dt} + B \cdot \omega_m + T_L \quad (2.4)$$

where:

J_M is the motor's moment of inertia

ω_m is the angular speed of the rotor

B is the friction coefficient of the motor

T_L is the load torque placed on the motor's shaft

The load torque T_L that is placed on the drive pulley which is mounted on the motor's shaft is expressed in Eqn. 2.5:

$$T_L = R_P \cdot F_L + J_P \frac{d\omega_m}{dt} \quad (2.5)$$

where:

R_P is the radius of the drive pulley

J_P is the inertia of the motor pulley

F_L is the force exerted on the drive pulley

If the elevator car is moving upwards the load force F_L is defined by Eqn. 2.6:

$$F_L = \frac{1}{2} \left[g \cdot (M_c - M_{cw}) + M_c \frac{du_c}{dt} \right] \quad (2.6)$$

where:

g is the gravitational constant

M_c is the mass of the car

M_{cw} is the mass of the counter-weight

u_c is the linear speed of the car

Eqn. 2.6 was derived for the elevator mechanical system shown in Fig. 2.5 in which the force exerted by the accelerating car F_C is split into two parts. One half acts on the belt attached firmly to the top of the elevator shaft and the other half acts on belt which is looped over the drive pulley. In a similar way the force exerted by the counter-weight is split into two parts, one half acting on the belt firmly attached to the top of the elevator shaft and one half acting on the belt which is looped over drive pulley. The belt which is driven by the drive pulley is moving with the speed u_b which is twice as great as the car speed u_c . This is expressed as:

$$u_b = 2u_c \quad (2.7)$$

The car speed expressed in terms of motor speed is expressed as:

$$u_c = \frac{1}{2} R_P \cdot \omega_m \quad (2.8)$$

The mechanical power of the car moving upwards with constant speed is:

$$P_{mc} = M_c \cdot g \cdot u_c \quad (2.9)$$

This power when written with respect to the pulling belt is:

$$P_{mb} = \frac{1}{2} M_c \cdot g \cdot u_b \quad (2.10)$$

Replacing the belt speed with the car speed, the power P_{mb} is shown to be:

$$P_{mb} = \frac{1}{2} M_c \cdot g \cdot 2 \cdot u_c = P_{mc} \quad (2.11)$$

Eqn. 2.11 shows that the power of the moving car is equal to the power of the pulling belt.

In Eqn. 2.6 the force F_L is affected by the gravitational force F_{Lg} and the inertia of the elevator car J_c , both of which are expressed as:

$$F_{Lg} = \frac{1}{2} \cdot g \cdot (M_c - M_{cw}) \quad (2.12)$$

$$J_c = \frac{1}{2} \cdot M_c \frac{du_c}{dt} \quad (2.13)$$

Eqn. 2.12 and Eqn. 2.13 hold only when the car is moving upwards and the belt is flexible; under these conditions the motor is not affected by the counter-weight during acceleration. With this assumption Eqn. 2.6 can be inserted into Eqn. 2.5. The load torque T_L is now expressed as:

$$T_L = \frac{1}{2} R_P \cdot g \cdot (M_c - M_{cw}) + \frac{1}{4} R_P^2 \cdot M_c \frac{d\omega_m}{dt} + J_P \frac{d\omega_m}{dt} \quad (2.14)$$

As mentioned, Eqn. 2.14 was derived for the elevator car moving upwards. When the elevator car accelerates moving downwards the counter-weight's mass M_{cw} should be considered while the elevator car's mass M_c should be ignored. The equation for load torque T_L when the elevator car is moving downwards has the form:

$$T_L = \frac{1}{2} R_P \cdot g \cdot (M_{cw} - M_c) + \frac{1}{4} R_P^2 \cdot M_{cw} \frac{d\omega_m}{dt} + J_P \frac{d\omega_m}{dt} \quad (2.15)$$

Substituting the load torque equation for when the elevator car is moving upwards (Eqn. 2.14) into the motor's motion equation (Eqn. 2.4), the motion equation of the entire system is obtained as:

$$T_{em} = \left(J_m + \frac{1}{4} R_P^2 \cdot M_c + J_P \right) \frac{d\omega_m}{dt} + B \cdot \omega_m + \frac{1}{2} R \cdot g \cdot (M_c - M_{cw}) \quad (2.16)$$

or:

$$T_{em} = J_{eq} \frac{d\omega_m}{dt} + B \cdot \omega_m + T_{Lg} \quad (2.17)$$

where the equivalent moment of inertia J_{eq} is:

$$J_{eq} = J_m + \frac{1}{4} \cdot R_P^2 \cdot M_c + J_P \quad (2.18)$$

and the load torque due to gravity T_{Lg} is:

$$T_{Lg} = \frac{1}{2} \cdot R_P \cdot g \cdot (M_c - M_{cw}) \quad (2.19)$$

With the equations describing the performance of the elevator and its electric drive known, attention can now be paid to the permanent-magnet DC motor itself. Chapter 3 extends the analysis of this thesis to the unique parameters of the electric drive which serves as the prime mover of the system.

Chapter 3: Determination of Parameters of Electric Elevator Drive

In order to correctly design position, speed, and current controllers for the elevator's electric drive, the parameters of the permanent-magnet DC Motor must first be determined. Parameters can vary from unit to unit and so each motor must have its unique values empirically determined. The mechanical and electrical characteristics of the permanent-magnet DC Motor are delineated as steady-state or dynamic values.

3.1 Steady-State Parameters

Steady-state characteristics of a permanent-magnet DC Motor reflect losses due to friction found in the electric drive and the relationship between electro-magnetic torque developed by the motor and the current drawn by the motor. The steady-state parameters to be determined are:

R_a - armature resistance

K – motor constant, relation between armature current and electro-magnetic torque

T_{fr} - static friction torque

B - motor friction coefficient

The relationship between the motor's supply voltage and its speed is linear and given by Eqn. 3.1.

$$V_a = R_a \cdot I_a + K \cdot \omega_m \quad (3.1)$$

which can be rearrange as:

$$\omega_m = \frac{V_a}{K} - I_a \frac{R_a}{K} \quad (3.2)$$

As seen in Fig. 3.1 this dependency can be expressed in y-intercept form as:

$$\omega_m = m \cdot I_a + c \quad (3.3)$$

where:

$$m = -\frac{R_a}{K} \quad (3.4)$$

$$c = \frac{V_M}{K} \quad (3.5)$$

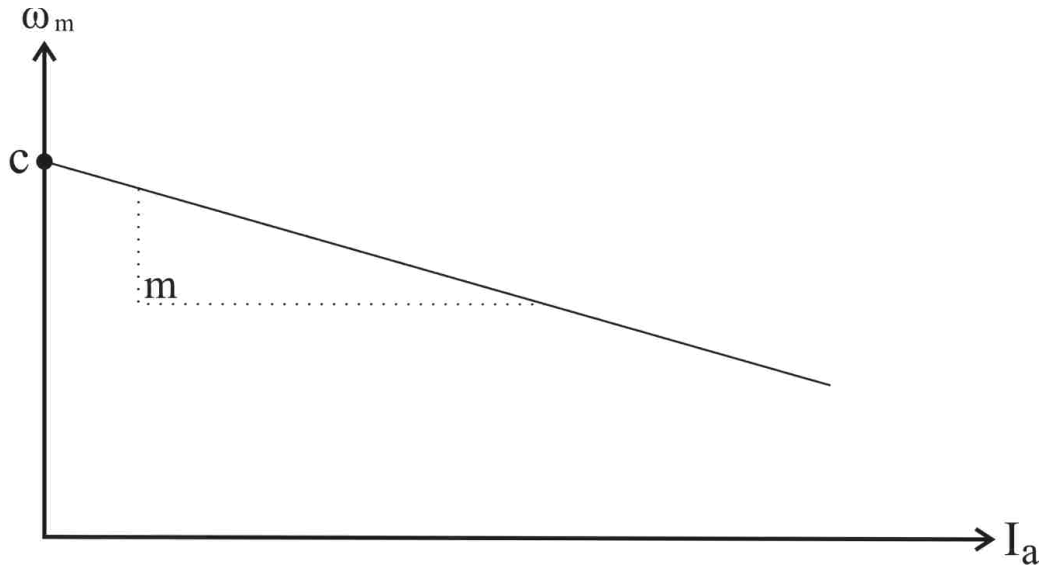


Figure 3.1 $\omega_m = f(I_a)$ Characteristic

To determine the parameters of the permanent-magnet DC motor in steady state, the Motor-Under-Test (MUT) will be axially coupled to another DC motor which will act as a load on the MUT. This arrangement is shown in Fig. 3.2 and a picture of the connected motors is shown in Fig. 3.3.

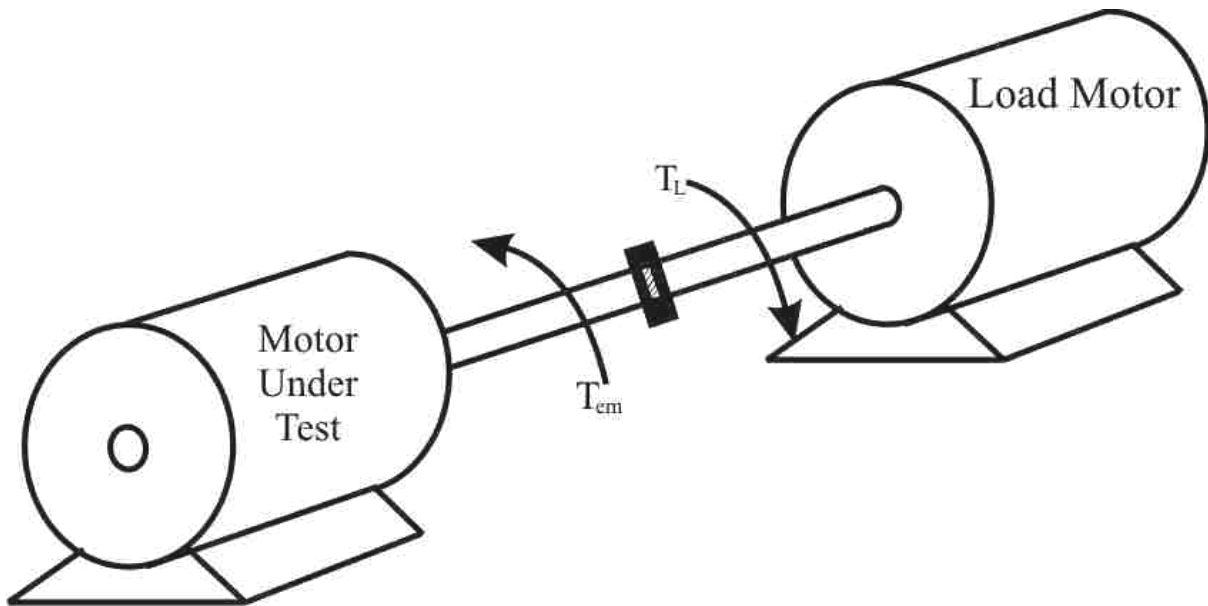


Figure 3.2 MUT connected to load motor



Figure 3.3 MUT axially coupled to load motor (seen in laboratory)

With the load motor's shaft rigidly attached to the shaft of the MUT, the supply voltages of the load motor and MUT are changed in incremental steps. The load torque T_L placed on the MUT is equal to the electro-magnetic torque developed by the load motor. At each step the speed, voltage, and current of the MUT are recorded until enough data points are collected to draw the speed-current characteristic [2]. The data points collected for 5 different MUT supply voltages are shown in Table 3.1 and the corresponding $\omega_m = f(I_a)$ characteristics are shown in Fig. 3.3.

For Table 3.1 the data points collected are:

V_M – voltage applied to MUT

V_L – voltage applied to load motor

I_M – current drawn by MUT

I_L – current drawn by load motor

ω_M – angular speed of MUT and load motor

Table 3.1 Steady-state parameter determination data

V_M [V]	5						10					
I_M [A]	0	1	2	3	4	5	0	1	2	3	4	5
V_L [V]	-6.00	-3.75	-2.00	-0.66	0.90	2.25	-11.75	-9.25	-7.20	-5.85	-4.25	-3.00
I_L [A]	-0.87	0.14	1.07	2.01	3.01	4.05	-1.02	0.03	1.06	1.91	2.92	3.87
ω_m [$\frac{rad}{s}$]	65	49	40	32	20	12	141	123	109	101	89	80

V_M [V]	15						20					
I_M [A]	0	1	2	3	4	5	0	1	2	3	4	5
V_L [V]	-17.20	-14.85	-12.75	-11.00	-9.60	-8.15	-22.20	-20.00	-18.20	-16.50	-15.00	-13.40
I_L [A]	-1.45	-0.16	0.82	1.86	2.75	3.66	-1.28	-0.22	0.67	1.51	2.27	3.22
ω_m [$\frac{rad}{s}$]	210	199	180	171	160	149	278	262	255	247	230	218

Table 3.1 Continued

V_M [V]	30					
I_M [A]	0	1	2	3	4	5
V_L [V]	-	-	-	-	-	-
	32.70	30.40	28.30	26.40	24.70	22.50
I_L [A]	-1.22	-0.29	0.68	1.56	2.43	3.35
ω_m [$\frac{rad}{s}$]	409	394	379	369	358	347

The data collected during the steady-state parameter test is plotted in Fig. 3.4 in a speed versus armature current fashion. For each voltage applied to the MUT, the speed versus current characteristic is linearized; the slope (m) and y-intercept (c) for each linearized characteristic is used to determine R_a and K for each voltage applied to the MUT. Rearranging Eqn. 3.4 and Eqn. 3.5, the value of K for each voltage V_M applied to the MUT can be calculated as:

$$K = \frac{V_M}{c} \quad (3.6)$$

and the value of R_a for each voltage V_M applied to the MUT can be calculated as:

$$R_a = -K \cdot m \quad (3.7)$$

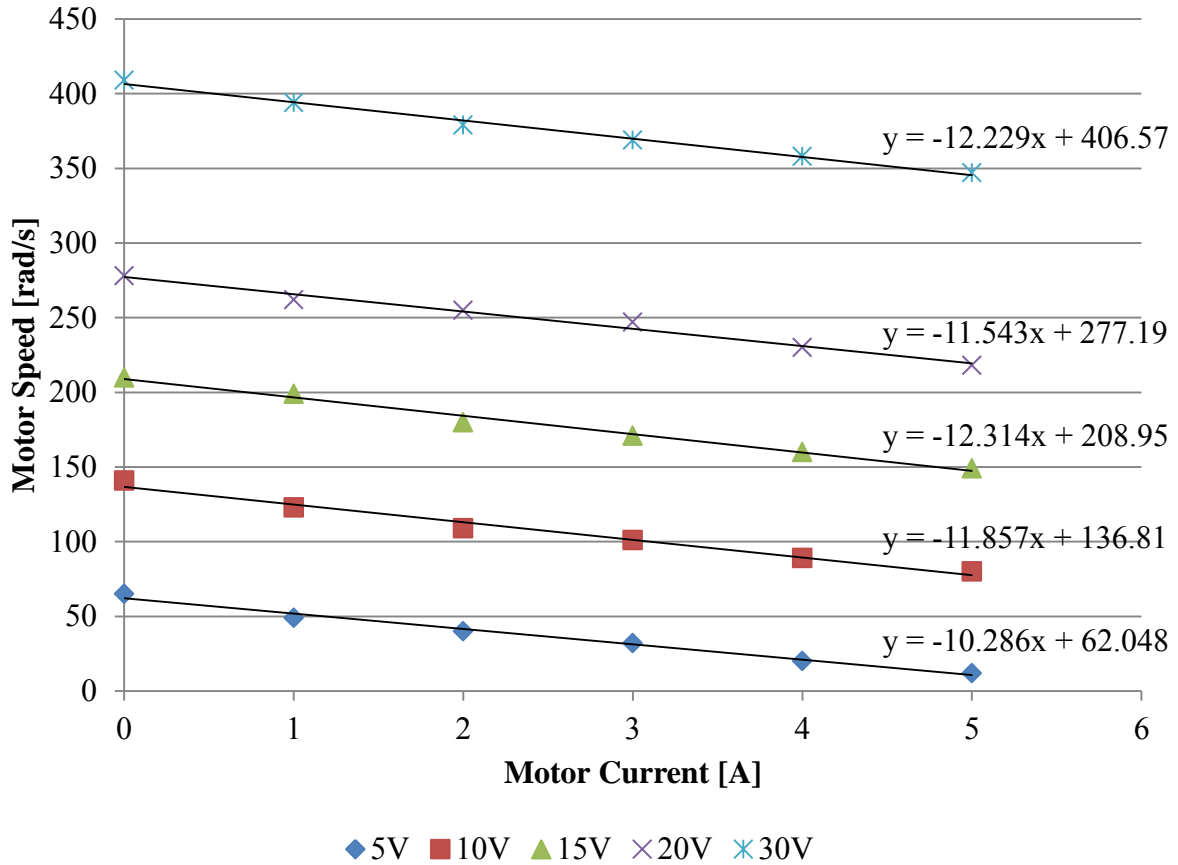


Figure 3.4 Speed versus armature current characteristics

Shown in Table 3.2 are the parameters derived from the $\omega_m = f(I_a)$ characteristics shown Fig. 3.4.

Table 3.2 Linearized data received from ω_m versus I_a characteristics

V_M [V]	m $\left[\frac{\text{rad}}{\text{s}/\text{A}}\right]$	c $\left[\frac{\text{rad}}{\text{s}}\right]$	K $\left[\frac{\text{V}}{\text{rad}/\text{sec}}\right]$	R_a [Ω]
5	-10.286	62.048	0.081	0.83
10	-11.857	136.81	0.073	0.87
15	-12.314	208.95	0.072	0.89
20	-11.543	277.19	0.072	0.83
30	-12.229	406.57	0.074	0.90

The average values are calculated as:

$$K = \frac{\sum_{i=1}^n K_i}{n}, c = \frac{\sum_{i=1}^n c_i}{n}, m = \frac{\sum_{i=1}^n m_i}{n}, R_a = \frac{\sum_{i=1}^n R_{a_i}}{n} \quad (3.8)$$

where $n = 5$ is the number of $\omega_m = f(i_a)$ characteristics as seen in Fig. 3.4.

The calculated average values obtained from the steady-state characteristics are shown in Table 3.3.

Table 3.3 Average values of motor parameters obtained from steady-state characteristics

m	c	K	R_a
$\left[\frac{\text{rad}}{\text{s}} / \text{A} \right]$	$\left[\frac{\text{rad}}{\text{s}} \right]$	$\left[\frac{\text{V}}{\text{rad/sec}} \right]$	$[\Omega]$
-11.646	218.314	0.0744	0.864

Friction in the permanent-magnet DC Motor consists of two components, one that is constant and one that is dependent on the speed of the motor. The first friction component is the static friction torque T_{fr} which is constant throughout the motor's range of operation. The second friction component is proportional to the motor speed [5]. The motor torque equation considering these two friction forces in steady-state operation is:

$$T_{em} = T_L + B \cdot \omega_m + T_{fr} \quad (3.9)$$

To determine the friction of the permanent-magnet DC Motor the motor will be operated without a load; unburdened the motor must only overcome static friction torque T_{fr} and the friction represented by the friction coefficient B . As an increasing voltage is applied to the motor terminals, the current through the motor and the speed of the motor shaft is recorded [2]. From the recorded current the torque produced by the motor can be calculated as:

$$T_{em} = K \cdot I_a \quad (3.10)$$

where:

$$K = 0.0744 \left[\frac{N \cdot m}{A} \right] \quad (3.11)$$

The data obtained from the no-load test is enclosed in Table 3.4.

Table 3.4 Steady-state friction determination data

V_M [V]	I_M [A]	ω_m $\left[\frac{rads}{s} \right]$	T_{em} [N · m]
5	0.344	59	0.0256
10	0.385	126	0.0286
15	0.415	193	0.0309
20	0.446	260	0.0332
25	0.475	328	0.0353
30	0.508	395	0.0378
35	0.546	462	0.0406
39	0.570	515	0.0424

The correlation between electro-magnetic torque and motor shaft speed is expressed as:

$$T_{em} = B \cdot \omega_m + T_{fr} \quad (3.12)$$

and can be expressed in y-intercept form where:

$$B = m \quad (3.13)$$

$$T_{fr} = c \quad (3.14)$$

The torque versus speed characteristic for the data contained in Table 3.4 is plotted in Fig. 3.5.

The y-intercept data obtained from the no-load characteristic shown in Fig. 3.5 is contained in Table 3.5.

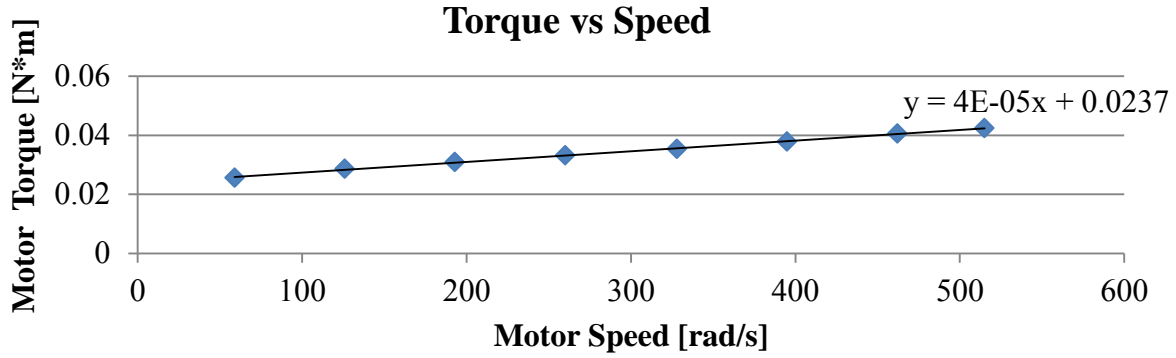


Figure 3.5 Torque-speed characteristic of steady-state friction model

Table 3.5 Steady-state friction parameters

m	c	B	T_{fr}
[slope]	[intercept]	$\left[\frac{N \cdot m}{rad/sec} \right]$	$[N \cdot m]$
0.00004	0.0237	0.00004	0.0237

3.2 Dynamic Parameters

Permanent-magnet DC motor dynamic parameter armature inductance, L_a is an element of the motor's electrical circuit and is a measure of resistance to change in the current flowing through the motor's armature circuit i_a . The dynamic parameter rotor moment of inertia, J_M is an element of the motor's mechanical assembly and is a measure of the motor's resistance to change in speed ω_m .

The dynamic equations for the permanent-magnet DC Motor are:

$$V_a = R_a \cdot i_a + K \cdot \omega_m + L_a \frac{di_a}{dt} \quad (3.13)$$

$$T_{em} = T_L + T_{fr} + B \cdot \omega_m + J \frac{d\omega_m}{dt} \quad (3.14)$$

Armature current i_a and angular speed ω_m are not independent of one another so both the armature inductance L_a and moment of inertia J will change with a variance in current or speed. To more easily determine the values of L_a and J , the variables i_a and ω_m are isolated from one another. With

the variables isolated, two experiments can be performed to determine the electrical and mechanical dynamic characteristics of the permanent-magnet DC motor.

To determine the inductance of the motor's armature circuit the rotor of the permanent-magnet DC motor is blocked so that it does not move ($\omega_m = 0$). A step voltage is applied to the armature winding so that the current increases exponentially with time until reaching the limit of $\frac{V_a}{R_a}$ (see Fig. 3.6) [2].

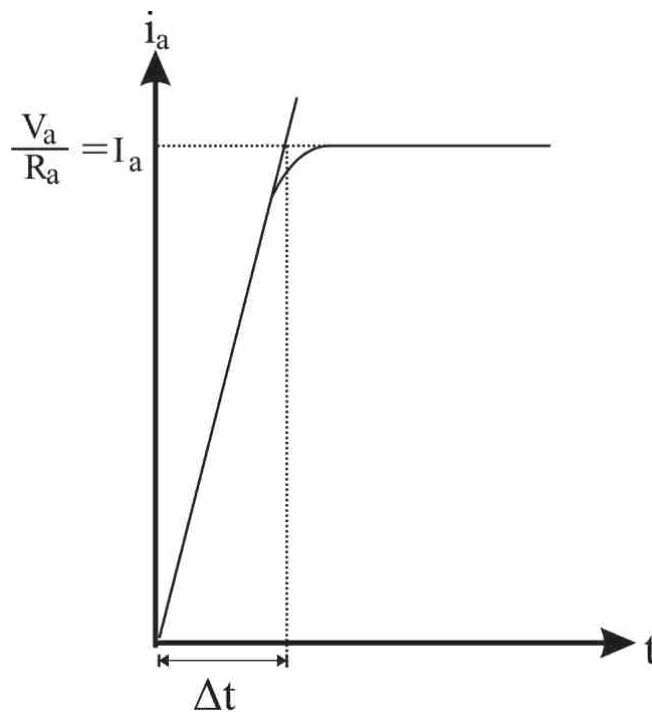


Figure 3.6 Current response with blocked rotor ($\omega_m = 0$)

When $\omega_m = 0$ the motor's voltage equation is:

$$V_a = R_a i_a + L_a \frac{d i_a}{dt} \quad (3.15)$$

which can be modified to find current:

$$i_a(t) = \frac{V_a}{R_a} (1 - e^{-\frac{t}{\tau_a}}) \quad (3.16)$$

where:

$$\tau_a = \frac{L_a}{R_a} \quad (3.17)$$

The slope of the curve as measured at $t = 0$ is dependent on L_a . This dependency can be expressed as:

$$\frac{V_a}{L_a} = \left(\frac{di_a}{dt} \right)_{t=0} \quad (3.18)$$

An examination of the current response during the blocked rotor test will reveal the armature inductance L_a to be:

$$L_a = \frac{V_a}{\left(\frac{di_a}{dt} \right)_{t=0}} \quad (3.19)$$

where the slope is:

$$\left(\frac{di_a}{dt} \right)_{t=0} = \frac{I_a}{\Delta t} \quad (3.20)$$

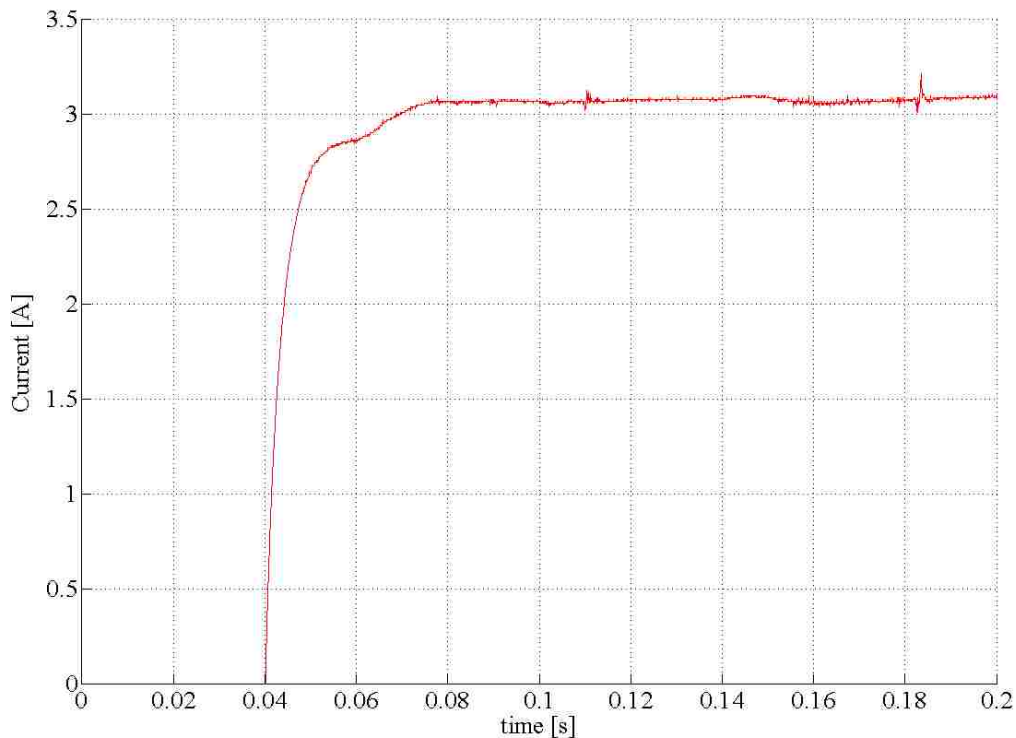


Figure 3.7 Current waveform for 3V step increase

The current curve obtained during the blocked rotor test is shown in Fig. 3.7. The results of the blocked rotor test are show in Table 3.6 and inductance L_a is found according to Eqn 3.19.

Table 3.6 Inductance of armature winding

Δt [s]	I_a [A]	V_a [V]	$\left(\frac{di_a}{dt}\right)_{t=0}$	L_a [H]
0.0109	3.07	3	281.651	0.0107

To properly determine the moment of inertia for the permanent-magnet DC Motor the effects of electro-magnetic torque must be negated. Disconnecting the motor's power supply will effectively eliminate current flow and reduce the corresponding electro-magnetic torque to zero. Before removing power from the system, the motor-under-test is brought up to the no-load speed ω_0 by a second motor such that current through the MUT is 0 and friction losses are compensated for by the alternate motor [2]. At $t = 0$ power is removed from both motors and both T_{em} and T_L become 0. The dynamic torque equation:

$$T_{em} = T_L + T_{fr} + B\omega_m + J\frac{d\omega_m}{dt} \quad (3.21)$$

becomes:

$$0 = T_{fr} + B\omega_m + J\frac{d\omega_m}{dt} \quad (3.22)$$

Once power is removed from the system the motor speed reduces exponentially with time and is expressed as:

$$\omega_m(t) = \left(\omega_0 + \frac{T_{fr}}{B}\right)e^{-\frac{B}{J}t} - \frac{T_{fr}}{B} \quad (3.23)$$

The speed function expressed by Eqn. 3.23 is illustrated in Fig. 3.8.

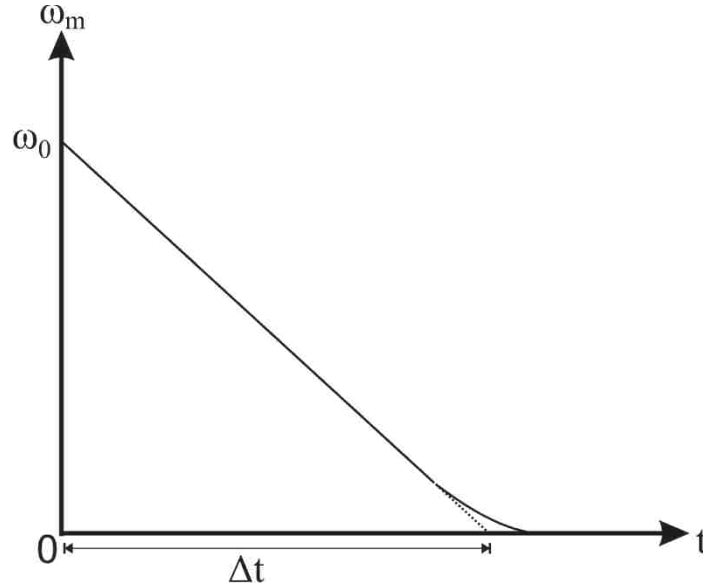


Figure 3.8 System speed response upon shutdown

The friction model is an approximation because the static friction torque T_{fr} is not always constant but dependent on speed [5]. Once the motor speed reaches 0, T_{fr} also reaches 0. Knowing this we can rearrange the above equation as:

$$\left(\omega(t) + \frac{T_{fr}}{B}\right) = \left(\omega_0 + \frac{T_{fr}}{B}\right) e^{-\frac{B}{J}t} \Rightarrow \Omega(t) = \Omega_0 e^{-\frac{B}{J}t} \quad (3.24)$$

Examining the above equation shows that by shifting the exponential curve with a constant value, the inertia is dependent on the slope of the curve at $t = 0$:

$$\left(\frac{d\Omega}{dt}\right)_{t=0} = \left(\frac{d\omega}{dt}\right)_{t=0} = -\Omega_0 \frac{B}{J} \quad (3.25)$$

The moment of inertia J can now be determined knowing ω_0 and B and graphically estimating the slope of the curve.

$$J = -\omega_0 \frac{B}{(\text{slope})_{t=0}} \quad (3.26)$$

where:

$$(\text{slope})_{t=0} = \frac{-\omega_0}{\Delta t} \quad (3.27)$$

The speed curve recorded during the test is shown in Fig. 3.9. The inertia of two motors J is determined with Eq. 3.26 using measurements taken from Fig. 3.9; this value must be halved to find the inertia of one motor J_M .

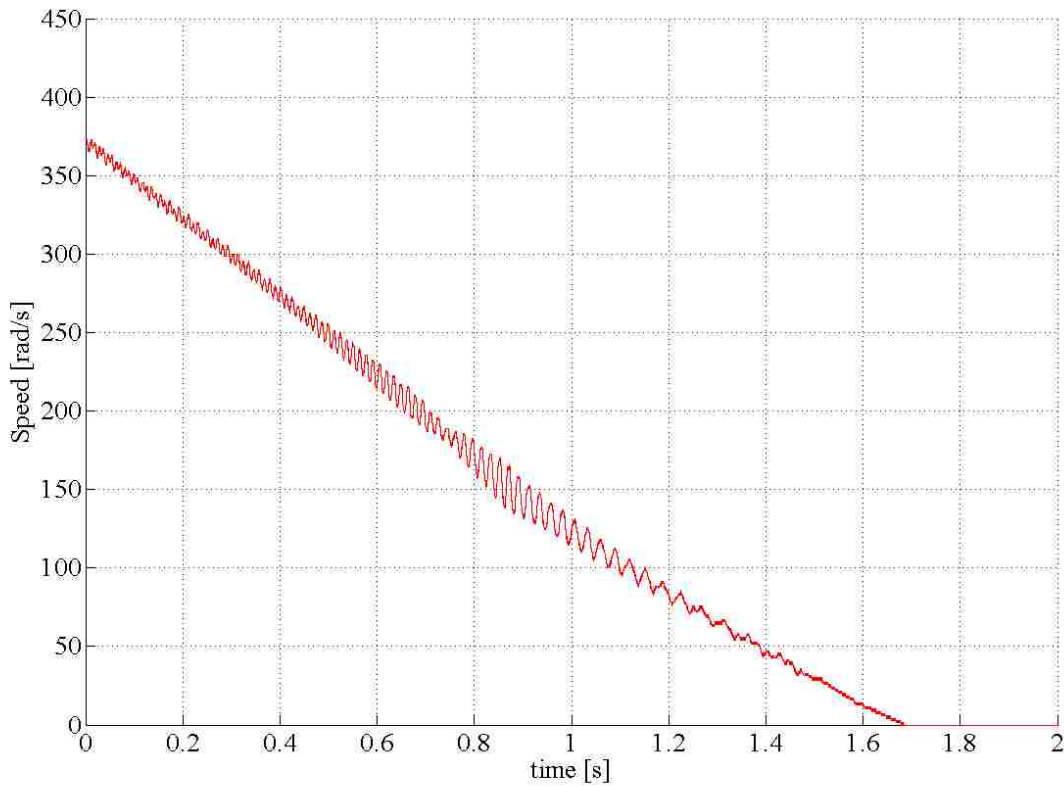


Figure 3.9 Speed response after power supply is disconnected from motors

The results of the no-load speed test are enclosed in Table 3.7.

Table 3.7 Results of equivalent inertia J_{eq} calculations

ω_0	Δt	J	J_M
$\left[\frac{rads}{s}\right]$	[s]	$[kg \cdot m^2]$	$[kg \cdot m^2]$
379	1.71	0.0002437	0.000122

The inertia of the motor and its load should be considered in the designing of the elevator's digital control system. This combined inertia can be found using Eqn. 3.28.

$$J_{eq} = J_M + \frac{1}{4}R_P^2 \cdot M_c + J_P \quad (3.28)$$

where:

J_M is the inertia of motor

R_P is the radius of drive pulley

M_c is the mass of elevator car

J_P is the inertia of the drive pulley

The inertia of the drive pulley J_P is calculated as [5]:

$$J_P = 4 \cdot J_M \quad (3.29)$$

The data for the permanent-magnet DC motor and attached drive system for which the equivalent inertia J_{eq} was calculated for is enclosed in Table 3.8 and the result of the calculation is contained with Table 3.9.

Table 3.8 Data for determination of equivalent inertia J_{eq}

J_M [kg · m ²]	R_P [m]	M_c [kg]	J_P [kg · m ²]	J_{eq} [kg · m ²]
0.000122	0.025	1.673	0.00487	0.000741

The position, speed, and current control loops can now be designed using the unique values attributed to the permanent-magnet DC motor which will be used for the elevator electric drive. The design of these cascaded control loops is covered in Chapter 4.

Chapter 4: Designing of Control System

The digital control system for implementation of position, speed, and current control of the elevator's electric drive is composed of three cascaded loops which are coordinated to work together using information obtained from the motor's position sensor and power supply's current output. Knowing the motor's steady-state and dynamic parameters the individual control loops are each designed to perform a specific task using a specific input. Using Matlab's Simulink software package these separate loops are integrated into one digital control system which is then compiled into machine language, loaded on the dSpace DS1104 hardware, and then executed in real time.

4.1 Feedback Control of Electric Drive

Feedback controllers are implemented with the goal of precisely and quickly regulating a system based upon real-time input obtained from the system itself without the need for correction from any outside observer. A properly designed control system will bring the steady-state error of a process to zero in a short time frame with few oscillations and minimum overshoot.

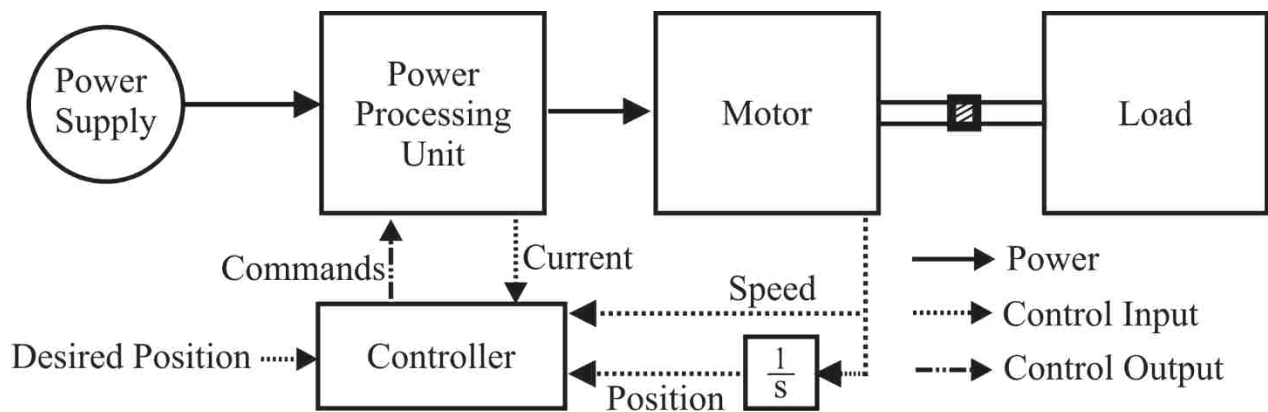


Figure 4.1 Feedback control system of DC motor

Fig. 4.1 is a block representation of the elevator's electric drive and feedback control system. A Direct Current (DC) power source is connected to the motor via a Power Processing Unit (PPU). The speed of the motor is captured by sensor and fed back to the controller. The position of the

motor is obtained by integrating the speed of the drive over time and is also fed back to the controller. The current flow out of the PPU is monitored and reported back to the controller as well. With these three real-time inputs the controller can bring the motor to the desired position. A closer examination of the controller block reveals three nested loops (see Fig. 4.2). Two loops contain a Proportional-Integral (PI) controller which is well suited to the task of regulating the electric drive's current and speed and one loop that contains a Proportional (P) controller which will adequately correct errors in the drive's position.

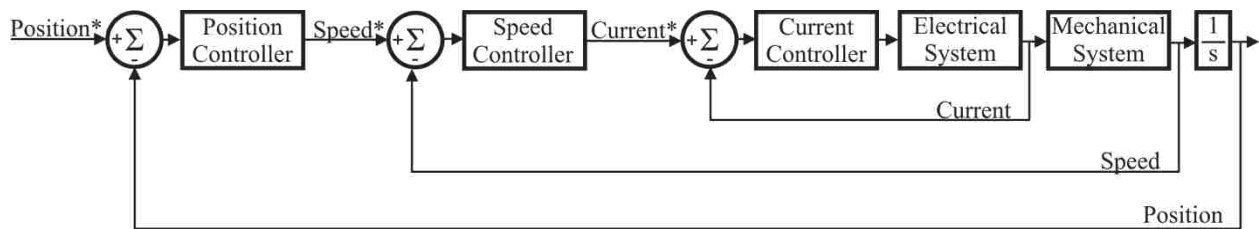


Figure 4.2 Cascaded control system

Shown in Fig. 4.3 is a diagram of a PI controller. The difference between the desired input $X^*(s)$ and the actual output $X(s)$ is known as the error $E(s)$. Two corrective values are generated from the error $E(s)$. The value $V_{c,p}(s)$ is the product of the error $E(s)$ and the gain k_p ; this provides a swift and proportional correction to system disturbances. The value $V_{c,i}(s)$ is the product of the error $E(s)$ and the gain k_i with the result being integrated over time; this provides a slow and gradual correction to counter system disturbances. The two corrective values, one to ensure the system adequately follows the desired reference value and one to reduce steady-state error, are summed and applied to the plant $G_p(s)$. The process's corrected output is compared to the reference input and the error $E(s)$ is recalculated, continuing the cycle indefinitely.

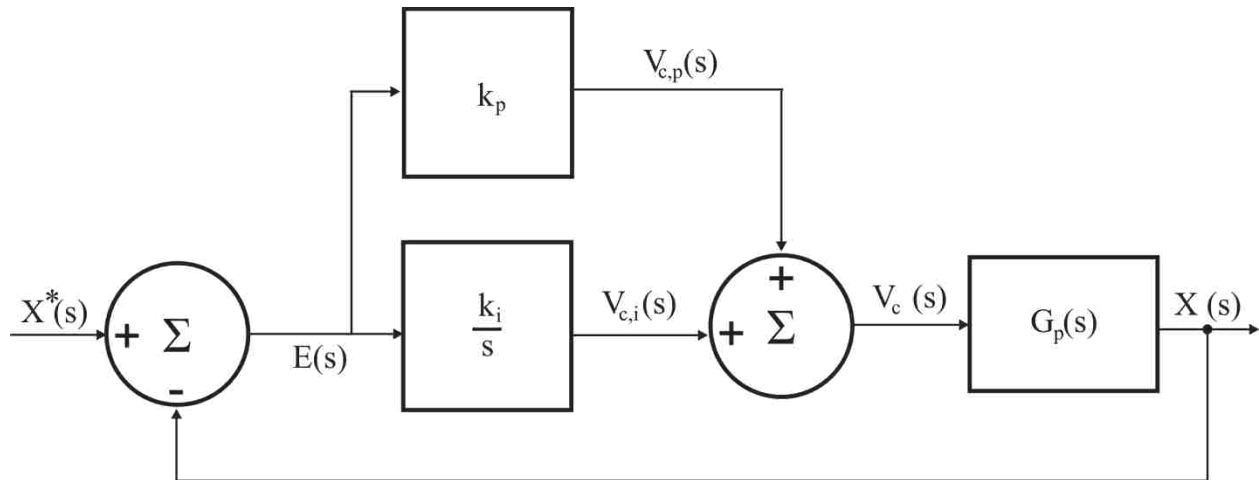


Figure 4.3 PI Controller Diagram

The error $E(s)$ which is fed into the PI controller can be expressed as:

$$E(s) = X^*(s) - X(s) \quad (4.1)$$

The proportional gain multiplies the error $E(s)$ times a constant k_p ; a larger error will produce a larger correction $V_{c,p}(s)$ and a small error will produce a smaller correction $V_{c,p}(s)$ as demonstrated in equation 4.2:

$$V_{c,p}(s) = k_p E(s) \quad (4.2)$$

The proportional gain acts in a linear fashion and can produce a steady-state error in response to a step-change so an integral gain is added to the controller so as to compensate for the proportional gain's deficiencies. By responding over time to the system's changing output the integral controller is able to gradually reduce the steady-state error to zero. The correction produced by the integral controller $V_{c,i}$ is expressed as:

$$V_{c,i} = \frac{k_i}{s} E(s) \quad (4.3)$$

A derivative gain is not used for the control of the elevator's electric drive because a derivative gain is susceptible to noise in the measurement system and could cause unwanted disturbances.

The open-loop transfer function of the PI controller seen in Fig. 4.2 is:

$$\frac{V_c(s)}{E(s)} = \left(k_p + \frac{k_i}{s}\right) = \frac{k_i}{s} \left[1 + \frac{s}{k_i/k_p}\right] \quad (4.4)$$

4.2 Current Control Loop

The current control loop is the innermost and fastest loop of the controller. The current control loop calculates the difference between the reference current and the current being supplied to the motor by the PPU. The reference current value is obtained from the output of the speed controller and the value of the current being supplied to the motor is obtained by sampling the PPU output in real-time using an analog-to-digital converter on the dSpace 1104 hardware.

Fig. 4.4 is a diagram of the current loop in its entirety. In addition to the PI controller, Fig. 4.4 includes the transfer function blocks which represent the armature winding and a transfer block which represents the mechanical system. The gain k_{PWM} represents the PPU. Also shown in the diagram are two feedback loops, one is the current feedback loop and the other loop which is dependent on the motor's speed accounts for the electro-motive force (emf) which opposes the armature voltage $V_a(s)$. To simplify the design considerations of the current loop's PI controller, the current loop is reduced.

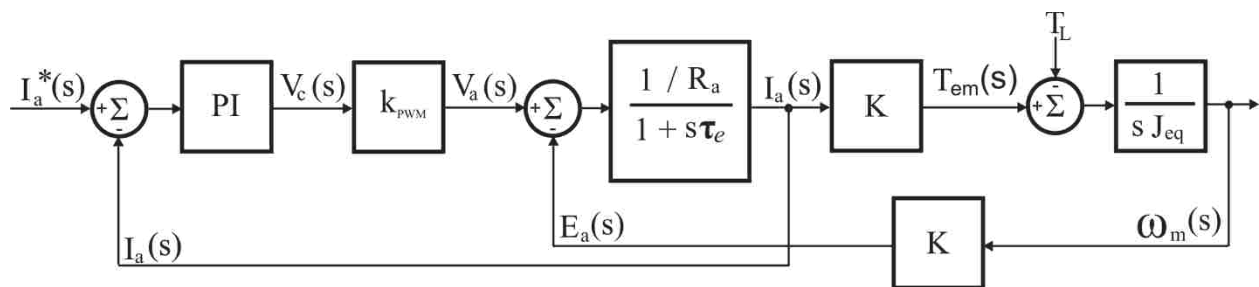


Figure 4.4 Expanded current control loop [6]

Fig. 4.5 is a diagram of the reduced current-loop shown in Fig. 4.4. To ease design considerations the load torque T_L is omitted and the induced back-emf $E_a(s)$ is calculated in terms of the current $I_a(s)$. The reduced current loop can be further simplified to stream-line the design of the current loop's PI controller.

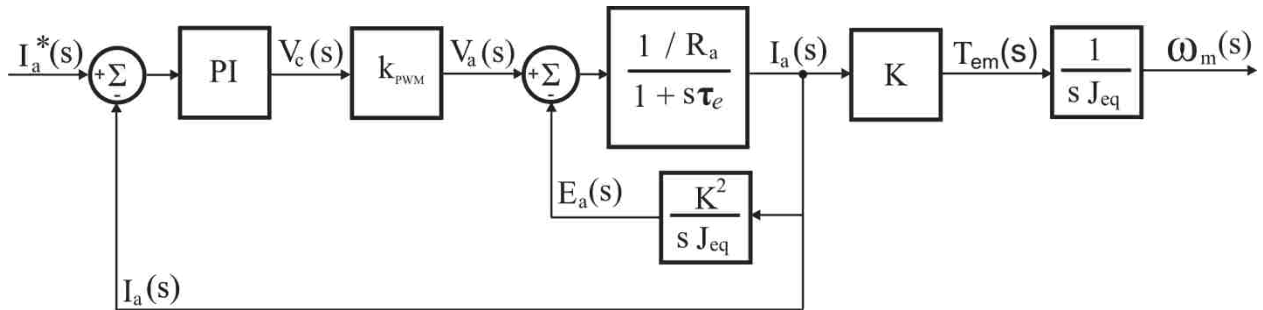


Figure 4.5 Reduced current control loop [6]

Fig. 4.6 is a diagram of the simplified current-loop shown in Fig. 4.5. Design considerations can be further reduced by assuming the equivalent inertia J_{eq} is sufficiently large enough to neglect the effects of the induced back-electro-motor force which is inversely dependent on said inertia. The transfer blocks representing the electro-magnetic torque of the motor and the speed of the motor can also be eliminated from the diagram as they are not included in the current feedback loop.

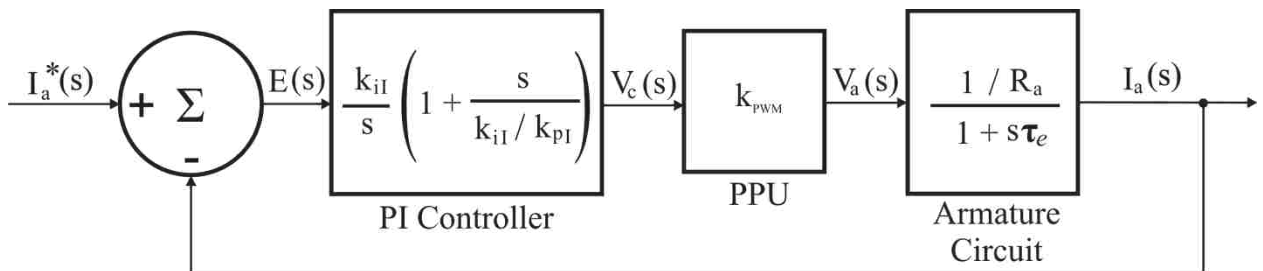


Figure 4.6 Simplified current control loop [6]

Fig. 4.6 shows the simplified current control loop of the permanent-magnet DC motor. The loop first determines the error between the reference current and the actual current flowing through the motor. This calculated error is used by the current control loop's PI controller to determine how the PPU's duty ratio must be changed in order to achieve a steady-state error of zero; the transfer function of the current control loop's PI controller is given by Eqn. 4.4. The modified control voltage $V_c(s)$ determined by the PI controller is multiplied by the gain of the 4-quadrant Pulse-Width-Modulation converter k_{PWM} to produce the voltage $V_a(s)$ which is applied to the motor's armature circuit. In Fig. 4.4 the permanent-magnet DC motor's armature circuit is represented by a simplified mathematical model and is expressed by the transfer function:

$$G_a(s) = \frac{1/R_a}{1+s\tau_e} \quad (4.5)$$

The open-loop transfer function of the simplified current control loop shown in Fig. 4.4 is:

$$G_{I,OL}(s) = \frac{k_{il}}{s} \left[1 + \frac{s}{k_{il}/k_{pl}} \right] \cdot k_{PWM} \frac{1/R_a}{1+s/\tau_e} \quad (4.6)$$

When designing the current control loop's PI controller, the gains k_{pl} and k_{il} are selected so as to achieve a phase margin of 90° for the controller. This is done by taking the open-loop transfer function of the current control loop (Eqn. 4.6) and setting the zero of the PI controller to cancel the motor pole as is done in Eqn. 4.7:

$$1 + \frac{s}{k_{il}/k_{pl}} = 1 + \frac{s}{1/\tau_e} \quad (4.7)$$

This leads to Eqn. 4.8:

$$\frac{k_{il}}{k_{pl}} = \frac{1}{\tau_e} \quad (4.8)$$

τ_e is the electrical time constant of motor which the time required for current to reach 63.2% of its final value at a fixed voltage level. The electrical time constant of the motor can be calculated as:

$$\tau_e = \frac{L_a}{R_a} \quad (4.9)$$

With the motor's pole canceled by the controller's zero, Eqn. 4.6 is reduced to:

$$G_{I,OL}(s) = \frac{k_{I,OL}}{s} \quad (4.10)$$

where:

$$k_{I,OL} = \frac{k_{il} \cdot k_{PWM}}{R_a} \quad (4.11)$$

Also, when designing the current control loop's PI controller the choice of crossover frequency f_{cl} is an important choice. The crossover frequency of the open-loop gain is chosen to be approximately one to two orders of magnitude less than the switching frequency of the PPU so that any noise from switching operations will not affect the current control loop's performance. The cross over frequency of the current loop f_{cl} is expressed in radians per second as:

$$\omega_{cl} = 2 \cdot \pi \cdot f_{cl} \quad (4.12)$$

The magnitude of the open-loop transfer function is equal to unity at the crossover frequency ω_{cl} :

$$|G_{I,OL}(j\omega_{cl})| = 1 \quad (4.13)$$

Thus following from Eqn. 4.10 and Eqn. 4.13, the gain of the integral controller k_{il} can be calculated as:

$$k_{il} = \frac{\omega_{cl} \cdot R_a}{k_{PWM}} \quad (4.14)$$

Knowing k_{il} , the gain of the proportional controller k_{pI} can be determined by rearranging Eqn. 4.8 as:

$$k_{pI} = k_{iI} \cdot \tau_e \quad (4.15)$$

The data for the permanent-magnet DC motor and PPU for which the current control loop was designed for is enclosed in Table 4.1 [1].

Table 4.1 Parameters for current control loop design

R_a	L_a	k_{PWM}	f_s	f_{ci}	ω_{ci}
[Ω]	[H]	[V]	[Hz]	[Hz]	$\left[\frac{rad}{s}\right]$
0.864	0.0107	40	2000	238	1495.4

The results of the k_{iI} and k_{pI} calculations are enclosed within Table 4.2

Table 4.2 Torque control loop integral gain calculations

k_{iI}	k_{pI}
32.3	0.40

4.3 Speed Control Loop

The cascaded control system's middle loop is the second fastest loop and dictates at what speed the electric drive should be turning. The speed control loop calculates the difference between the reference speed and the actual speed of the drive which is obtained from a sensor mounted on the motor's shaft. This calculated error in speed is manipulated by the speed loop's PI controller to produce a reference current value for the current control loop. Choosing a crossover frequency for the speed control loop that is at least one order of magnitude less than the crossover frequency of the current control loop reduces design constraints and ensures the nested loops do not conflict with one another. For the purpose of designing the speed control loop the closed current-loop is assumed to be ideal and is represented as a unity gain.

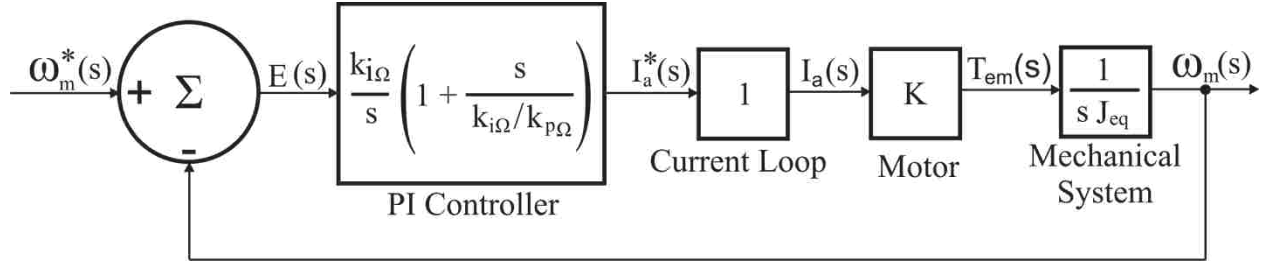


Figure 4.7 Simplified current control loop

The open-loop transfer function of the speed loop shown in Fig. 4.7 is:

$$G_{\Omega,OL}(s) = \frac{k_{i\Omega}}{s} \left[1 + \frac{s}{k_{i\Omega}/k_{p\Omega}}\right] \cdot 1 \cdot \frac{K}{s J_{eq}} \quad (4.16)$$

where:

$k_{i\Omega}$ is the integral gain of the speed controller

$k_{p\Omega}$ is proportional gain of the speed controller

Combining terms, Eqn. 4.16 can be rearranged as:

$$G_{\Omega,OL}(s) = \left(\frac{k_{i\Omega} \cdot K}{J_{eq}}\right) \frac{1+s/(k_{i\Omega}/k_{p\Omega})}{s^2} \quad (4.17)$$

An examination of Eqn. 4.17 shows that the open-loop transfer function contains a double pole at the origin. At low frequencies this double pole at the origin reduces the magnitude of the transfer function at a rate of -40db per decade while the phase angle is at -180°. This effect can be mitigated by choosing a crossover frequency that is at least one order of magnitude smaller than the crossover frequency of the current control loop and by choosing a phase margin of 60°. At the crossover frequency $\omega_{c\Omega}$ Eqn. 4.17 yields Eqn. 4.18 and Eqn. 4.19:

$$G_{\Omega,OL}(s) = \left(\frac{k_{i\Omega} \cdot K}{J_{eq}}\right) \frac{1+s/(k_{i\Omega}/k_{p\Omega})}{s^2} \Bigg|_{s=j\omega_{c\Omega}} = 1e^{j\phi_{OL,\Omega}} \quad (4.18)$$

$$-\frac{k_{i\Omega} \cdot K}{J_{eq} \cdot \omega_{c\Omega}^2} - j \frac{k_{i\Omega} \cdot K}{J_{eq} \cdot \omega_{c\Omega}} = 1[\cos(\phi_{pm,\Omega} - 180) + j \sin(\phi_{pm,\Omega} - 180)] \quad (4.19)$$

From Eqn. 4.19 the integral gain $k_{i\Omega}$ is:

$$-\frac{k_{i\Omega} \cdot K}{J_{eq} \cdot \omega_{c\Omega}^2} = \cos(\phi_{pm} - 180^\circ) \quad (4.20)$$

which can be rearranged as:

$$k_{i\Omega} = -\frac{J_{eq} \cdot \omega_{c\Omega}^2}{K} \cos(\phi_{pm} - 180^\circ) \quad (4.21)$$

and the proportional gain $k_{p\Omega}$ is:

$$-\frac{k_{i\Omega} \cdot K}{J_{eq} \cdot \omega_{c\Omega}} = \sin(\phi_{pm} - 180^\circ) \quad (4.22)$$

which can be rearranged as:

$$k_{p\Omega} = -\frac{J_{eq} \cdot \omega_{c\Omega}}{K} \sin(\phi_{pm} - 180^\circ) \quad (4.23)$$

The data for the permanent-magnet DC motor and attached elevator for which the speed control loop was designed for is enclosed in Table 4.3.

Table 4.3 Parameters for speed control loop design

K	J_{eq} [kg · m ²]	ϕ_{pm} [°]	$f_{c\Omega}$ [Hz]	$\omega_{c\Omega}$ [$\frac{rad}{s}$]
0.0744	0.000741	60	20	125.644

The results of the $k_{i\Omega}$ and $k_{p\Omega}$ calculations are enclosed within Table 4.4

Table 4.4 Results of speed loop gain calculations

$k_{i\Omega}$	$k_{p\Omega}$
78.639	1.084

4.4 Position Control Loop

The control system's outer loop is the slowest loop and ensures the elevator's electric drive is at the desired set point. The position of the drive's shaft and the connected elevator is determined by integrating the drive's speed; this is the same speed value which is fed back to the speed control loop. From the integrated speed, the position control loop determines the error between the desired set point and the actual position of the drive and reduces this error in position by changing the value of the reference speed. The position control loop's crossover frequency must be an order of magnitude less than that of the speed control loop which must be less than that of the current control loop's crossover frequency. For the purpose of designing the position control loop the closed speed-loop is assumed to be ideal and is represented as a unity gain. The position control loop is different from the speed and current loops in that it only has a proportional gain. The use of an integrator to obtain position from the speed data will reduce the steady-state error to zero for a step-change in the reference position.

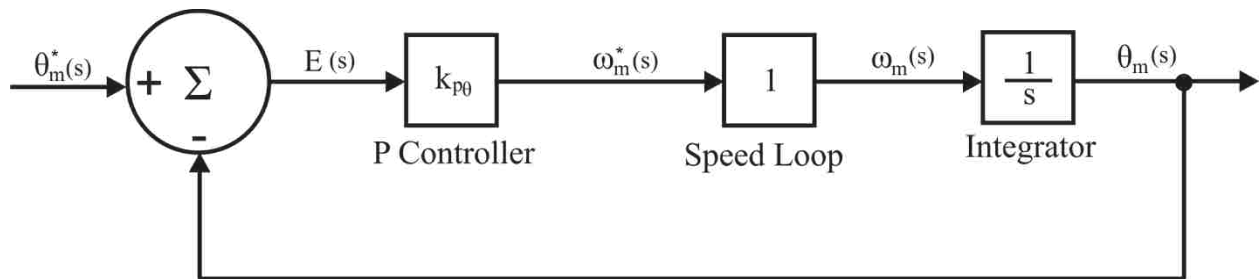


Figure 4.8 Position control loop block diagram

The open-loop transfer function of the position control loop shown in Figure 4.8 is:

$$G_{\theta,OL}(s) = \frac{k_{p\theta}}{s} \quad (4.24)$$

where $k_{p\theta}$ is the proportional gain of the position controller.

At the cross-over frequency the transfer function for the position controller is:

$$G_{\theta,OL}(j\omega_{c\theta}) = \frac{k_{p\theta}}{j\omega_{c\theta}} = 1e^{j\phi_{OL,\theta}} \quad (4.25)$$

Since from Eqn. 4.25

$$\phi_{OL,\theta} = -90^\circ \quad (4.26)$$

The phase margin $\phi_{PM,\theta}$ can be found as:

$$\phi_{PM,\theta} = \phi_{OL,\theta} + 180^\circ = 90 \quad (4.27)$$

The cross-over frequency is selected to be 1 Hz, hence the value of the gain shown in Table 4.5

Table 4.5 Position loop proportional gain calculations

$f_{c\theta}$ [Hz]	$\omega_{c\theta}$ [rad/s]	$k_{p\theta}$
1	6.283	6.283

With the design of the cascaded control system accomplished, the performance of the electric elevator drive can be examined. Chapter 5 covers the initial computer simulation of the DSP control and permanent-magnet DC motor as well as the experimental testing and results obtained in the laboratory.

Chapter 5: Performance of Electric Elevator Drive with Position Control

Upon determining the parameters of the permanent-magnet DC motor and designing the cascaded control system, a model of the system is created in Matlab's Simulink package. This model is used to simulate and observe the expected behavior of the system. Once the desired response is obtained during simulation the elevator electric drive with position control can be implemented in real time. The Simulink model used for simulation is modified to accept input and output from the dSpace 1104 hardware and then compiled into machine code which can be loaded on to the dSpace 1104 hardware. Position commands are issued from the Control-Desk software and the drive's response can be visually observed in addition to position data being collected by the dSpace 1104 hardware from the permanent-magnet DC motor's position encoder. Actual performance of the elevator's electric drive is compared against the simulated performance of the elevator's electric drive and observations are made as to how adequate the position control of the elevator's electric drive is. Each of these steps will be conducted by students in the course on electric machines so that they may experience the development of position control systems for electric drives.

5.1 Performance of Simulated Electric Elevator Drive with Position Control

For computer simulation the permanent-magnet DC motor parameters determined in Chapter 3 and the cascaded control system designed in Chapter 4 are used to build a Simulink model in Matlab which mimics the performance of the actual physical model.

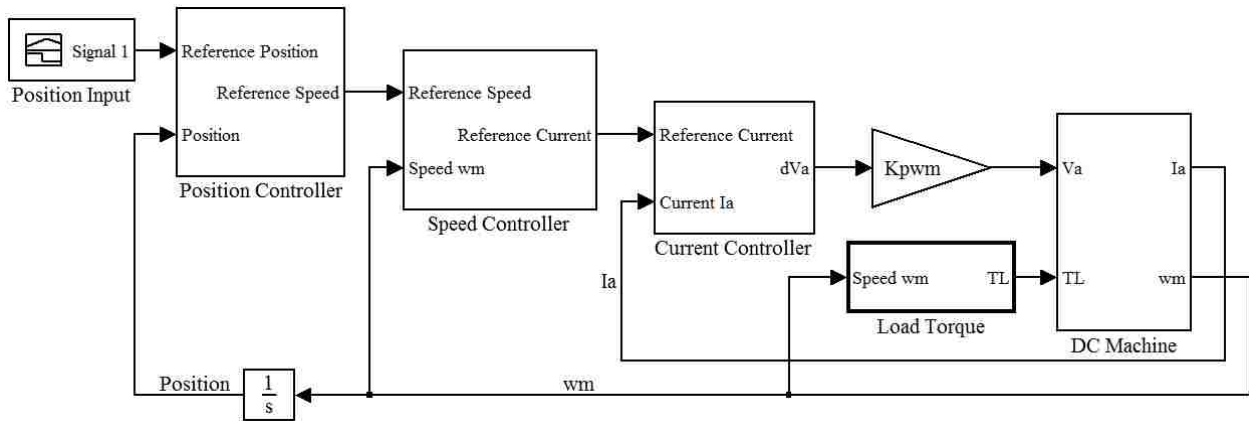


Figure 5.1 Simulink model of elevator electric drive with position control

Fig. 5.1 shows the cascaded control system and DC drive constructed in Matlab's Simulink allowing for simulation of the elevator's electric drive position control. Contained within this model is a subsystem which emulates the permanent-magnet DC motor used to drive the system in addition to the position, speed, and current control subsystems; the load torque placed on the permanent-magnet DC motor is determined within its on subsystem. The position input is generated by a signal block which produces a step change in reference position. Also seen in Fig. 5.1 is an integrator which obtains position from the mechanical speed of the motor and also seen is the gain k_{PWM} which represents the gain of the PPU. The PPU's output voltage V_a is the product of the DC power supply's voltage and the duty-ratio dV_a generated by the current controller. The block diagram seen in Fig. 5.2 is a graphical representation of Eqn. 5.1 and Eqn. 5.2.

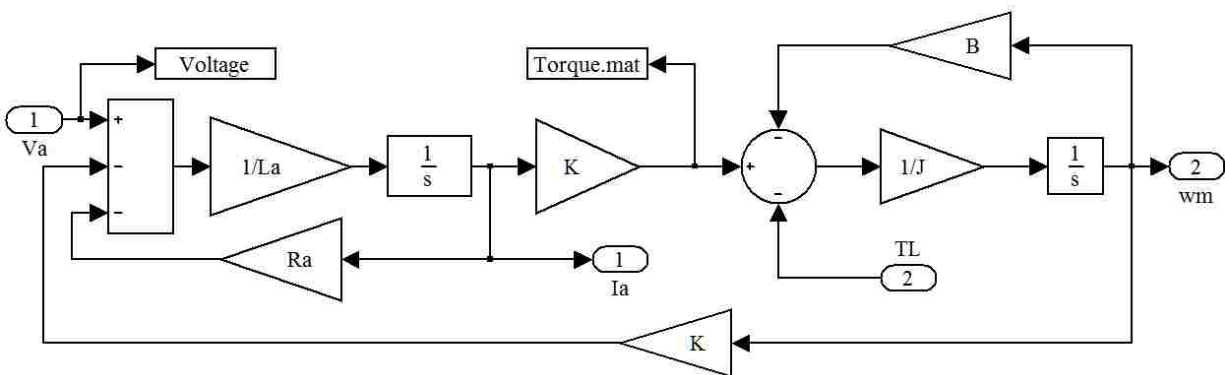


Figure 5.2 Simulated DC machine subsystem

$$I_a(s) = \frac{V_a(s) - E_a(s)}{R_a + sL_a} \quad (5.1)$$

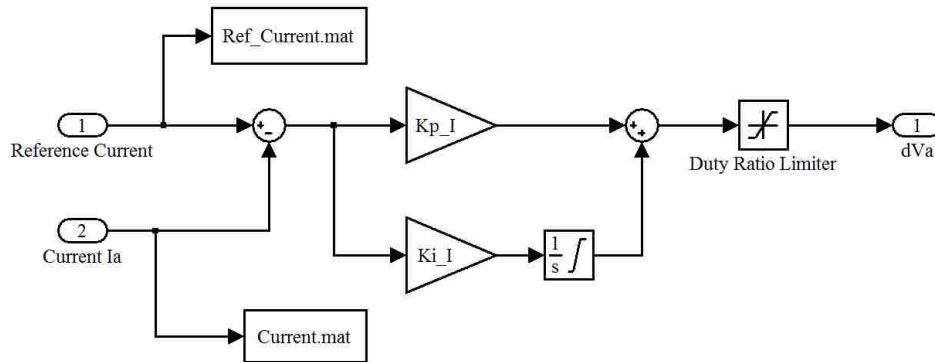
$$\omega_m = \frac{T_{em}(s) - T_L(s)}{sJ_{eq}} \quad (5.2)$$

where:

$$E_a(s) = K \cdot \omega_m(s) \quad (5.3)$$

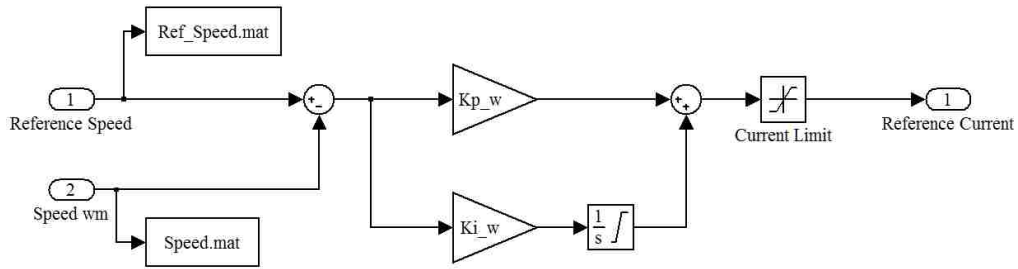
$$T_{em}(s) = K \cdot I_a(s) \quad (5.4)$$

The position, speed, and current control loops which were designed in Chapter 4 are each contained within their own subsystem. Each control subsystem calculates the error between the reference value and the actual value. Each control subsystem also contains the appropriate proportional and integral gains in addition to a saturation block which accounts for physical limitations such as the maximum current output of the power supply or the maximum speed at which the elevator can safely operate. Fig. 5.3 shows the current controller and Eqn. 5.6 describes its output. Fig. 5.4 shows the speed controller and Eqn. 5.7 describes its output. Fig. 5.5 show the position controller and Eqn. 5.8 describes its output. Eqns. 5.7, 5.8, and 5.9 notate the reference value by use of an asterisk (*).



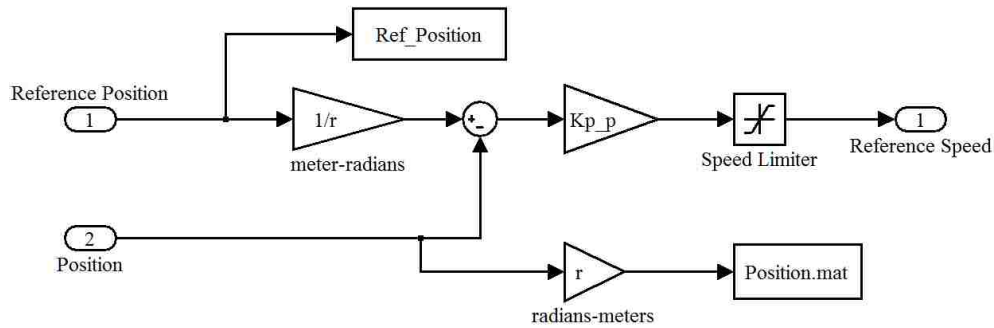
$$dV_a = (I_a^* - I_a)(k_{pI} + \frac{k_{iI}}{s}) \quad (5.5)$$

Figure 5.3 Simulated current controller subsystem



$$I_a^* = (\omega_m^* - \omega_m)(k_{p\Omega} + \frac{k_{i\Omega}}{s}) \quad (5.6)$$

Figure 5.4 Simulated speed controller subsystem

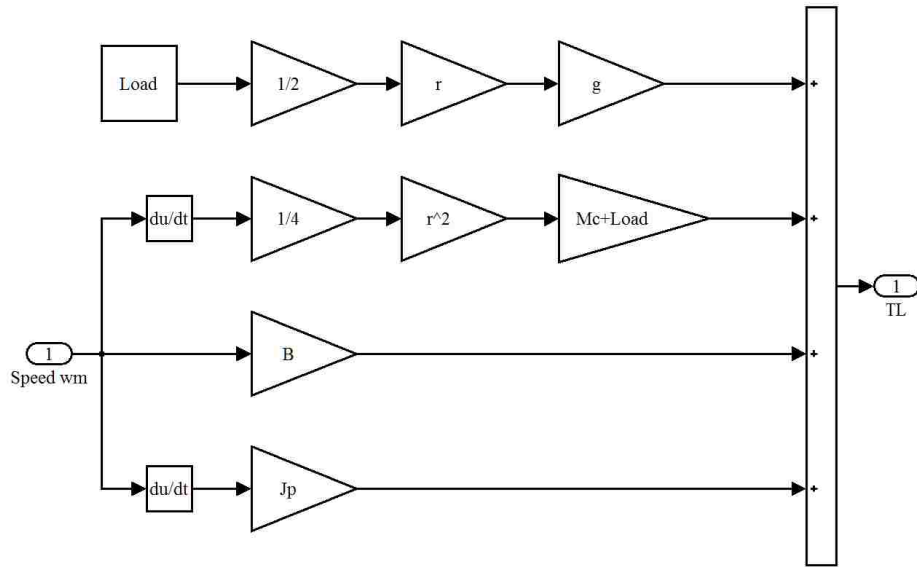


$$\omega_m^* = (\theta^* - \theta)k_{p\theta} \quad (5.7)$$

Figure 5.5 Simulated position controller subsystem

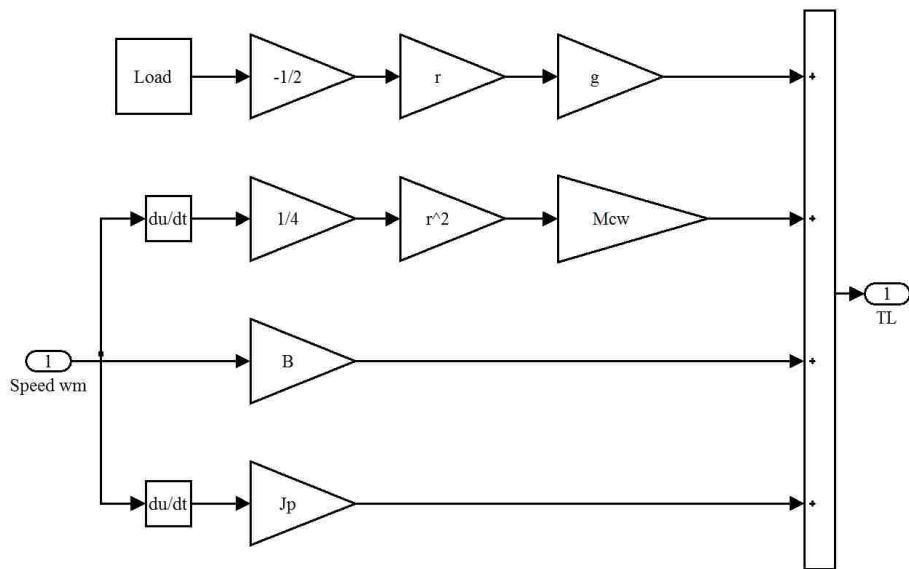
The load torque placed on the drive is a function of the drive's speed and the mass of the load placed in the elevator car; the mass of the elevator car and the mass of the counterweight are equal so only the mass of the object placed within the elevator car shall be considered "the Load". According to Eqn. 5.9 and Eqn. 5.10 (which were derived in Chapter 2, see Eqn. 2.14 and Eqn. 2.15) the calculation of load torque for the upwards motion is different from that of the downwards motion, for this reason the load torque subsystem for the ascending elevator car is different from the load torque subsystem for the descending elevator car. For the upward motion, the load's mass is added to the total load torque as a function of increased car mass and increased load inertia. For the downward motion, the load's mass detracts from the total load torque and the load's inertia is not considered as

only the counter-weight's inertia is considered. These similar yet different subsystems are illustrated in Fig. 5.6 and Fig. 5.7 with their corresponding equations.



$$T_L = \frac{1}{2} R \cdot g \cdot (\text{Load}) + \frac{1}{4} R^2 \cdot M_c \frac{d\omega_m}{dt} + B \cdot \omega_m + J_P \frac{d\omega_m}{dt} \quad (5.8)$$

Figure 5.6 Simulated load torque subsystem for ascending elevator car



$$T_L = -\frac{1}{2} R \cdot g \cdot (\text{Load}) + \frac{1}{4} R^2 \cdot M_{cw} \frac{d\omega_m}{dt} + B \cdot \omega_m + J_P \frac{d\omega_m}{dt} \quad (5.9)$$

Figure 5.7 Simulated load torque subsystem for descending elevator car

During simulation the position reference signal is generated using a signal builder block which produces a step change in desired height over time. This step input emulates the desired position change by a button press as elevators in the real world often have a button for each floor. Fig. 5.8 shows the elevator car rising from 0 to a height of 1 meter. Fig. 5.9 shows the elevator car descending from a height of 1 meter to 0.

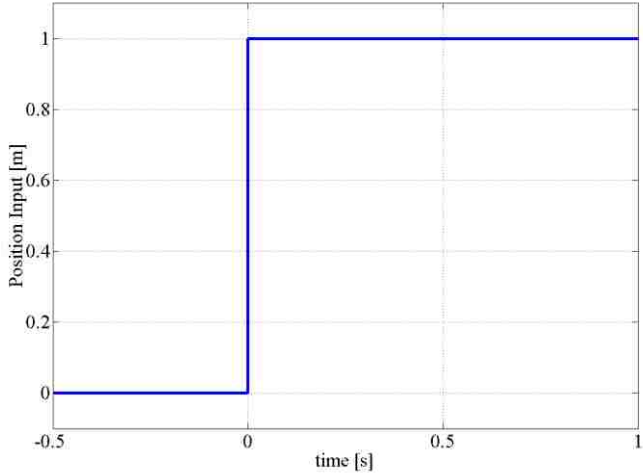


Figure 5.8 Simulated reference position of elevator electric drive with ascending car

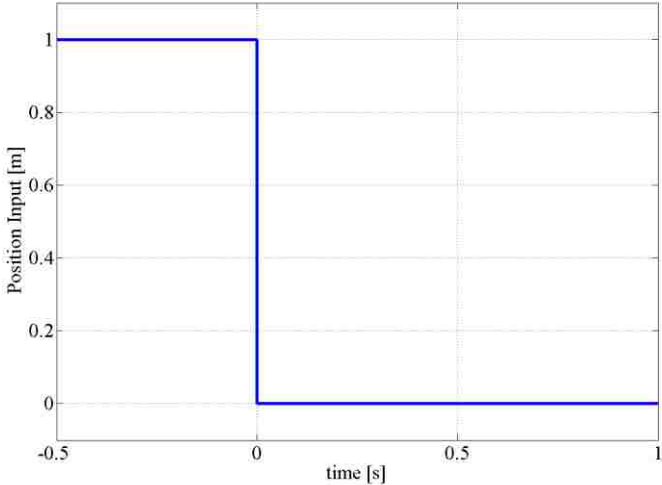


Figure 5.9 Simulated reference position of elevator electric drive with descending car

The response of the elevator electric drive for the elevator car containing a 1kg load is shown in Fig. 5.10 through Fig 5.19 for both the ascending and descending motions.

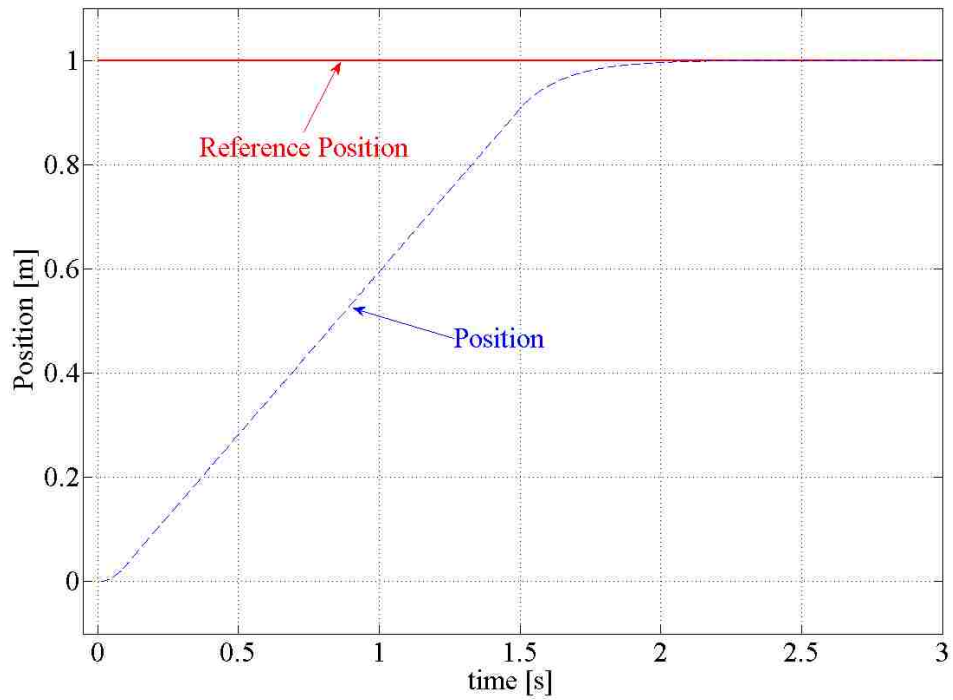


Figure 5.10 Simulated position response of elevator electric drive with ascending car

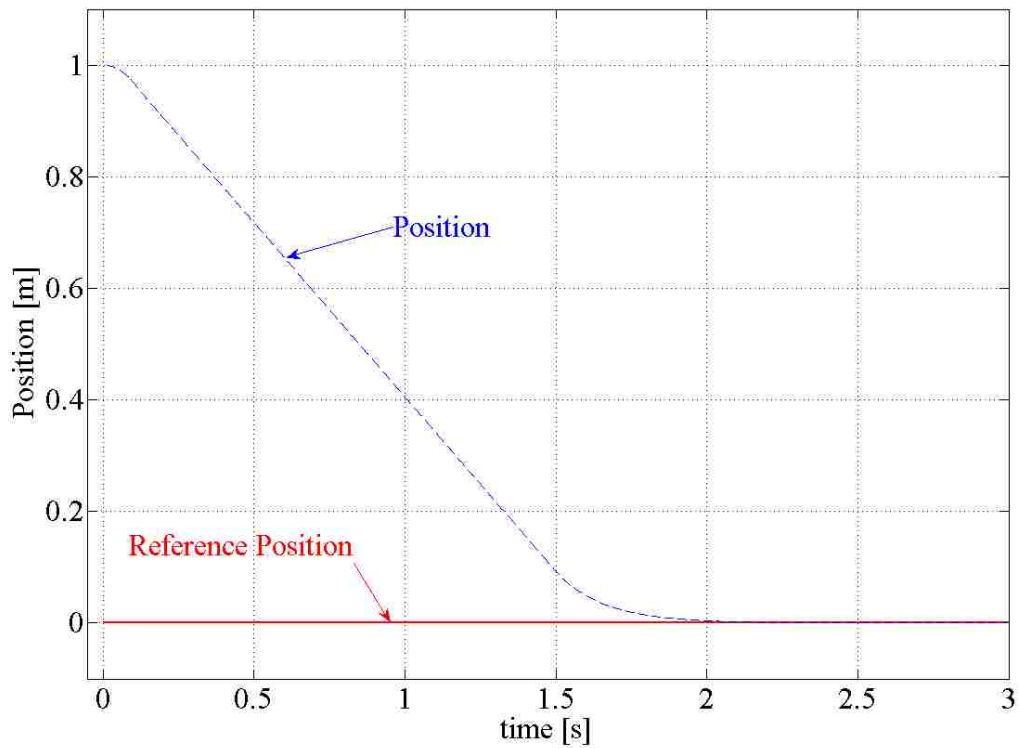


Figure 5.11 Simulated position response of elevator electric drive with descending car

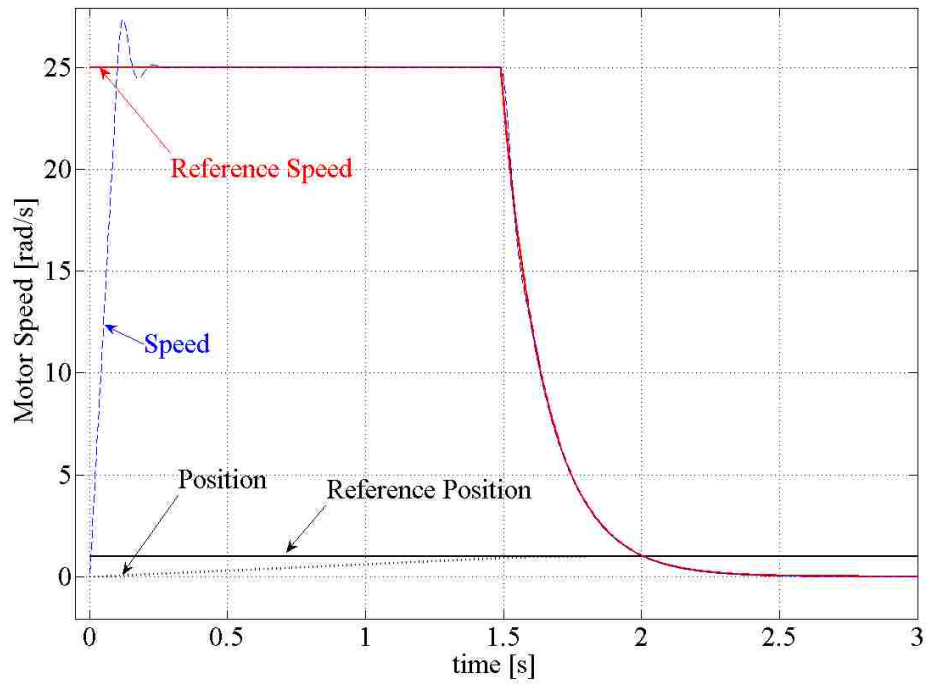


Figure 5.12 Simulated speed response of elevator electric drive with ascending car

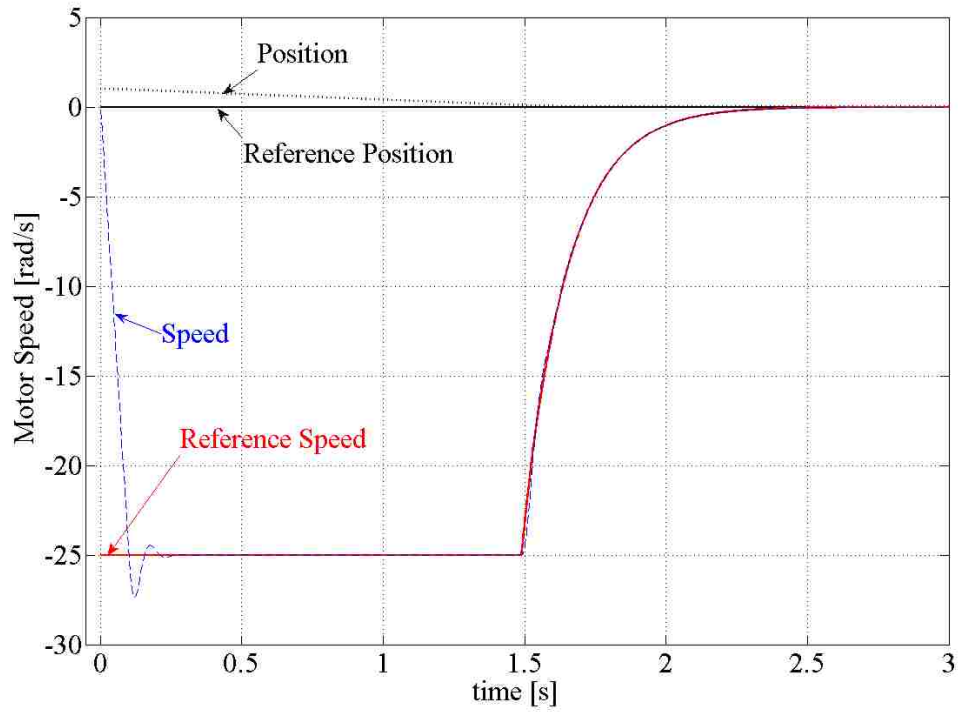


Figure 5.13 Simulated speed response of elevator electric drive with descending car

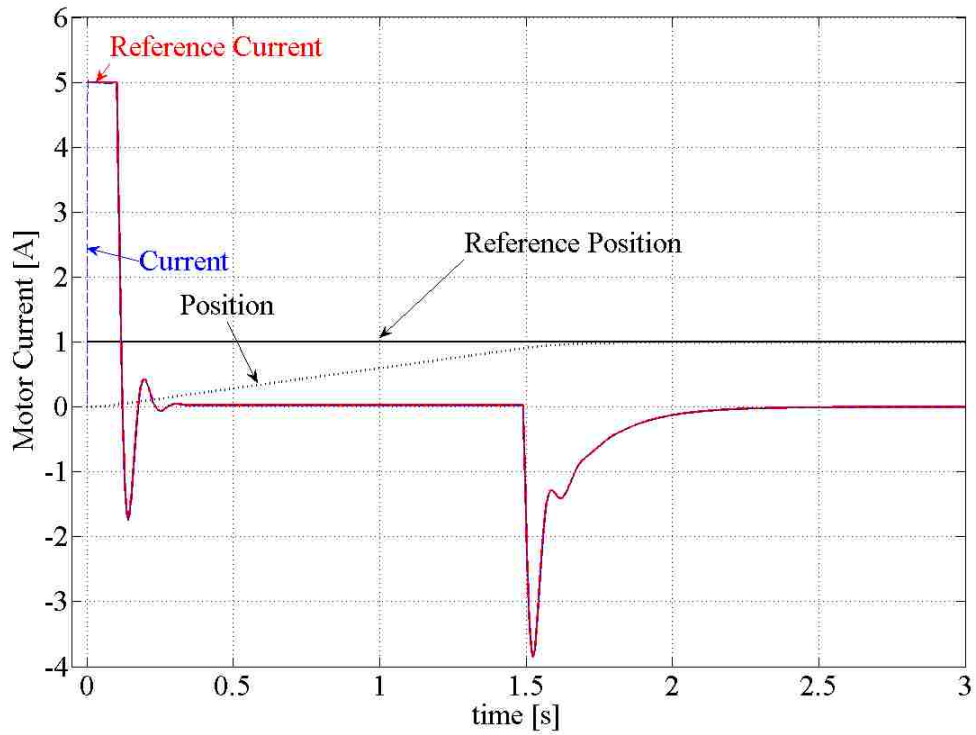


Figure 5.14 Simulated current response of elevator electric drive with ascending car

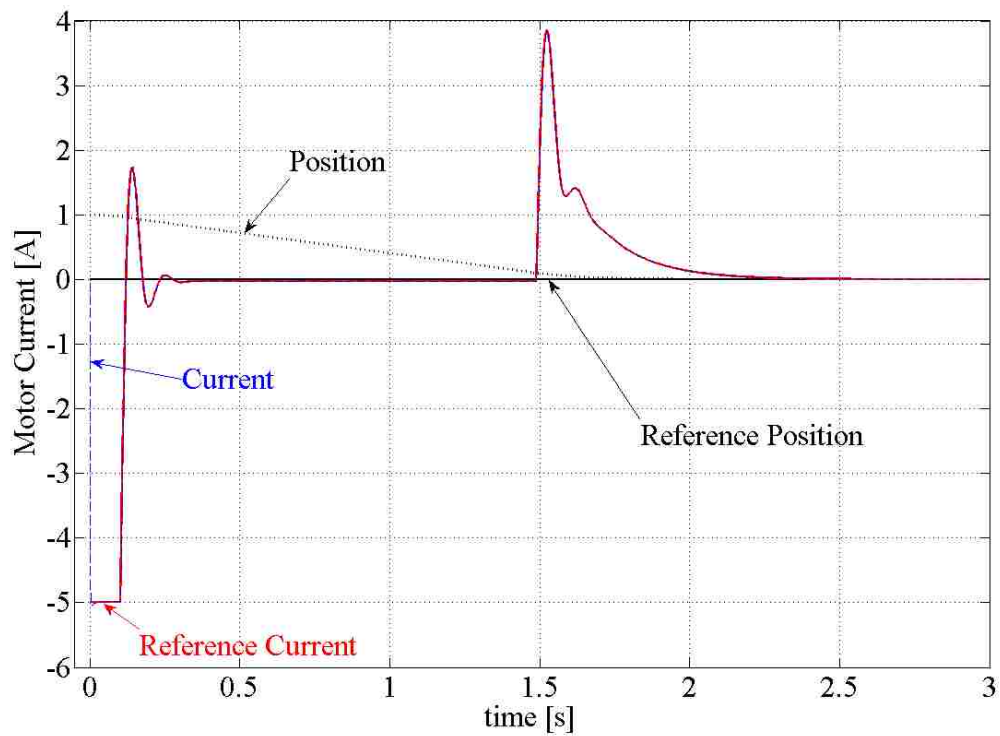


Figure 5.15 Simulated current response of elevator electric drive with descending car

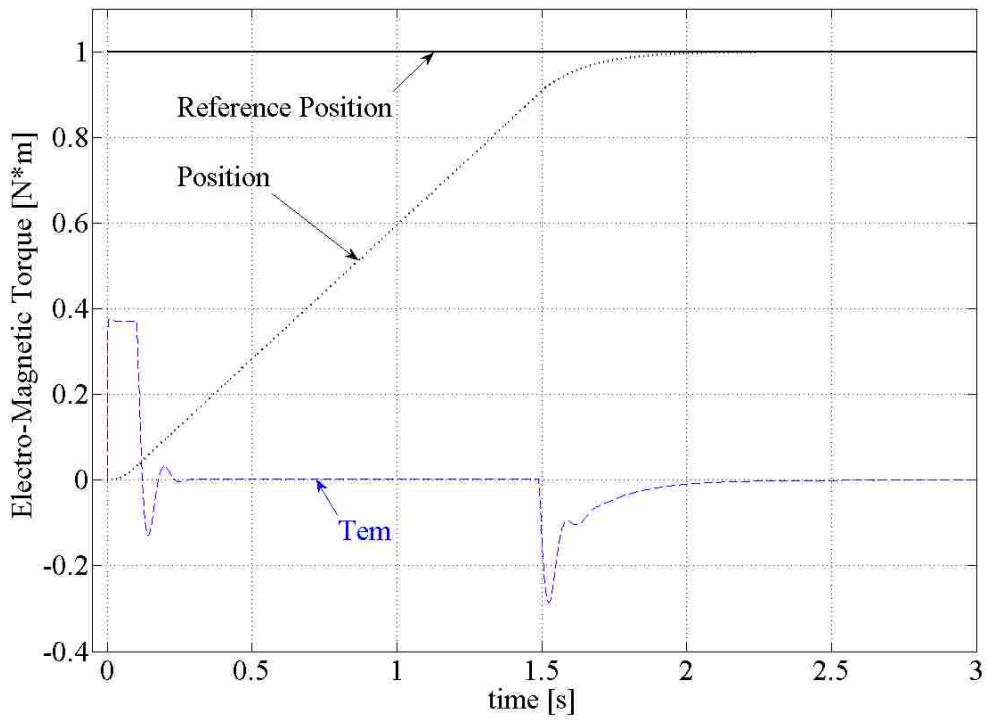


Figure 5.16 Simulated torque response of elevator electric drive with ascending car

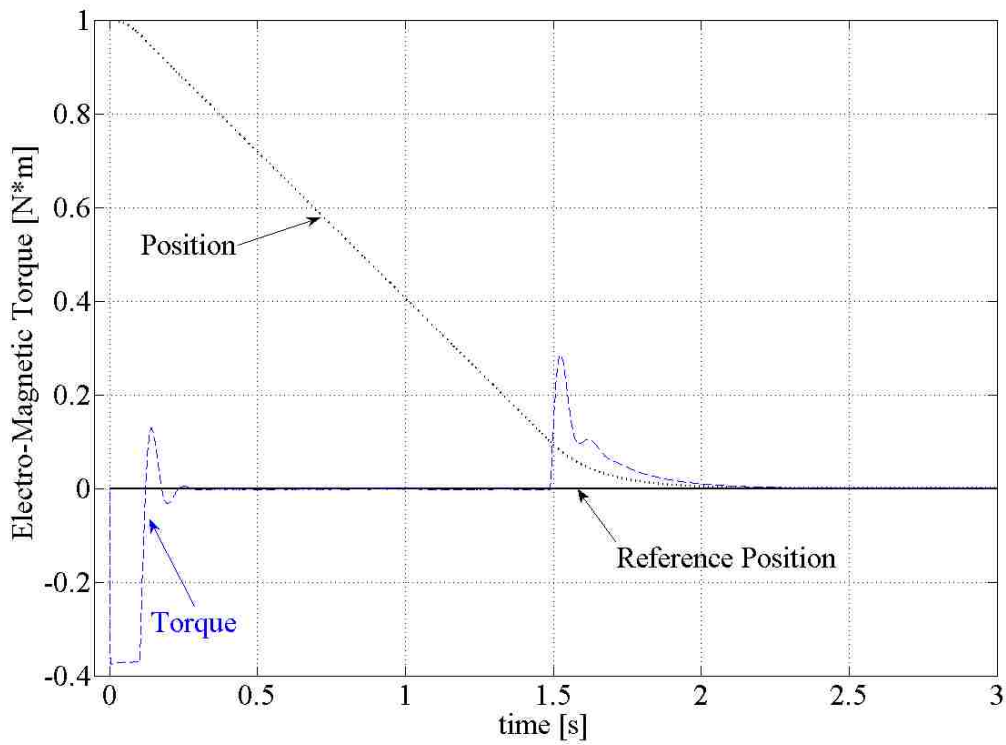


Figure 5.17 Simulated torque response of elevator electric drive with descending car

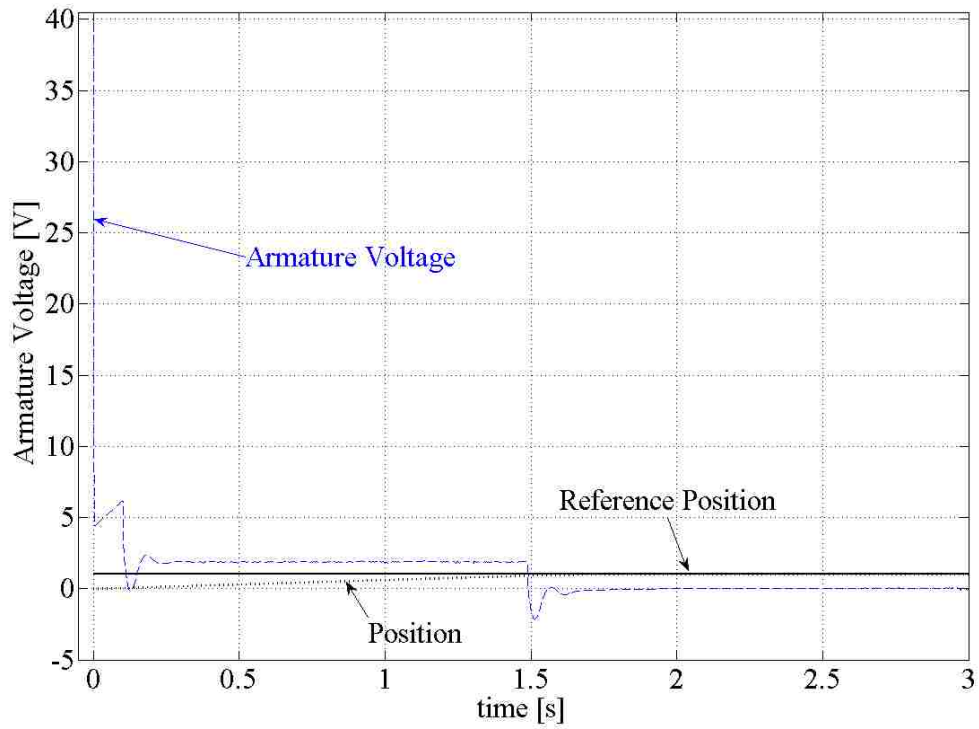


Figure 5.18 Simulated voltage response of elevator electric drive with ascending car

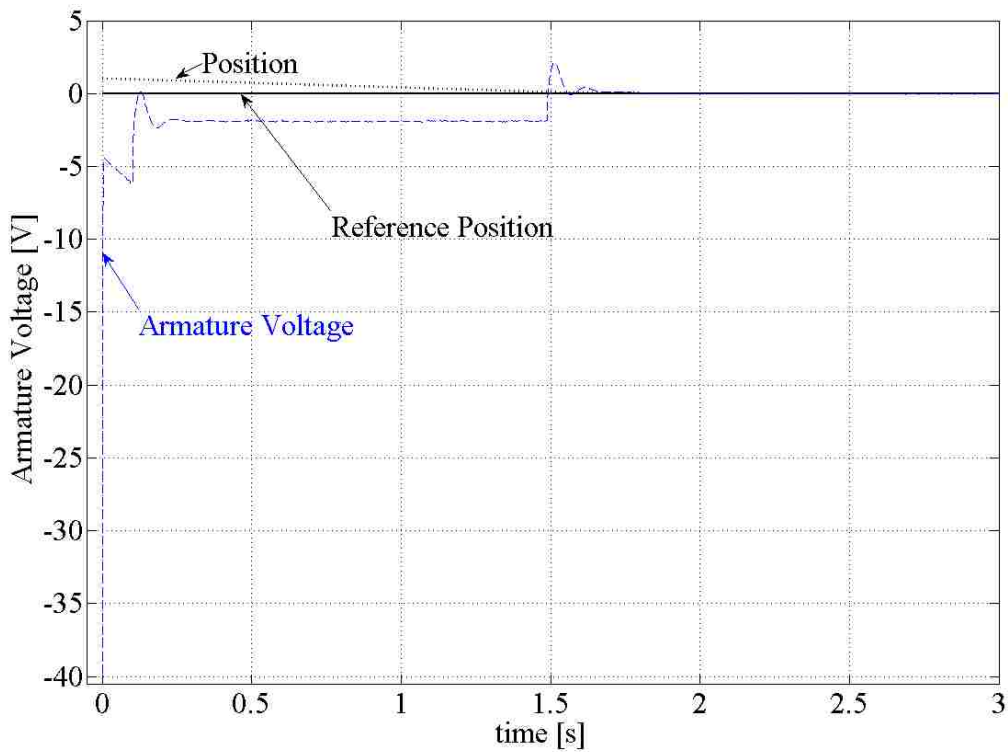


Figure 5.19 Simulated voltage response of elevator electric drive with descending car

From Fig. 5.10 and Fig. 5.11 it is observed that the elevator is able to move a load a distance of one meter in under three seconds. The speed at which the elevator changes position is shown in Fig. 5.12 and Fig. 5.13. Starting from a stand-still, the motor must overcome inertia and cannot immediately meet the reference speed issued by the speed controller; instead the motor accelerates to and temporarily exceeds the speed limit before settling at its maximum reference value of $25\frac{rad}{s}$ - this temporary overshoot in speed causes a rise in the voltage applied to the motor's terminal by the PPU (see Fig. 5.18 and Fig. 5.19) as it counters the back-emf e_a . As the elevator car approaches the desired position the reference speed decreases exponentially to zero and the elevator car comes smoothly to a stop. The current response to the step-change in position is immediate (see Fig. 5.14 and Fig. 5.15) as is the electro-magnetic torque produced by the motor (see Fig. 5.16 and Fig. 5.17). The PPU's ability to instantaneous switch on (see Fig. 5.18 and Fig. 5.19) ensures that current through the motor follows closely with the reference current value. To generate the maximum amount of torque at start-up, the reference current is at its maximum value until the motor's speed matches the reference speed at which point current through the motor is reversed to obtain braking torque in order to prevent the elevator car from accelerating beyond the speed limit. During steady-state operation current remains nearly zero as only friction and gravitational forces must be overcome. As the elevator car approaches the desired set point the motor must once again overcome inertia but in the opposite way as before. To start reducing the speed of the car a braking torque is applied; this torque starts at its maximum value and diminishes exponentially as kinetic energy is bled off from the system. Current once again returns to zero as the car glides smoothly to a stop and the system remains at rest. This process is repeated three times for no load, 1kg load, and 2kg load; the position response under these conditions is shown in Fig. 5.20 and Fig. 5.21.

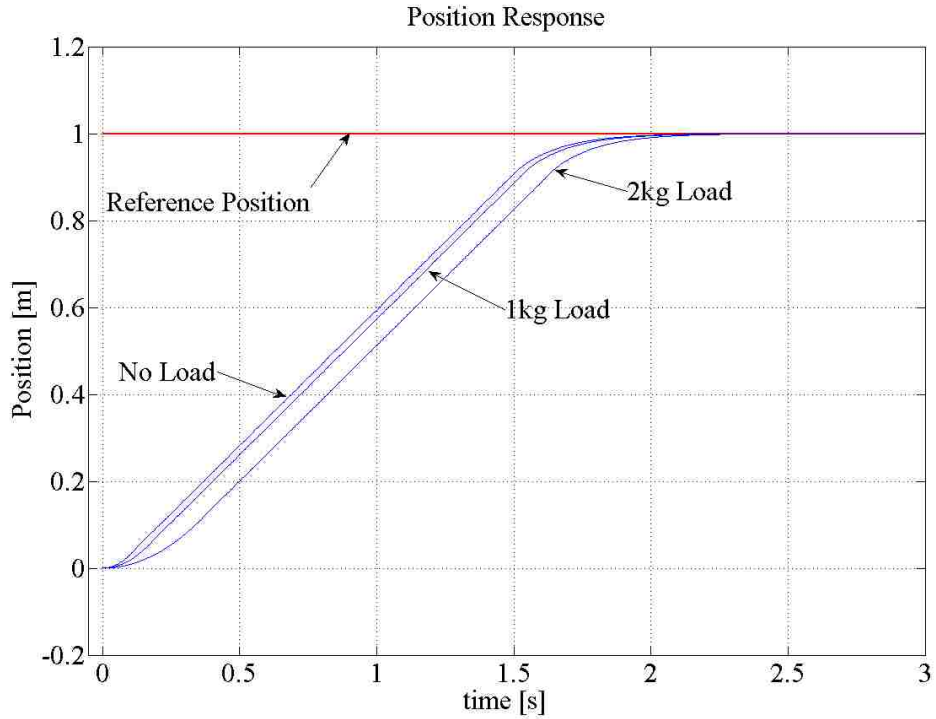


Figure 5.20 Simulated position response of elevator electric drive for ascending car carrying no load, 1kg load, and 2kg load.

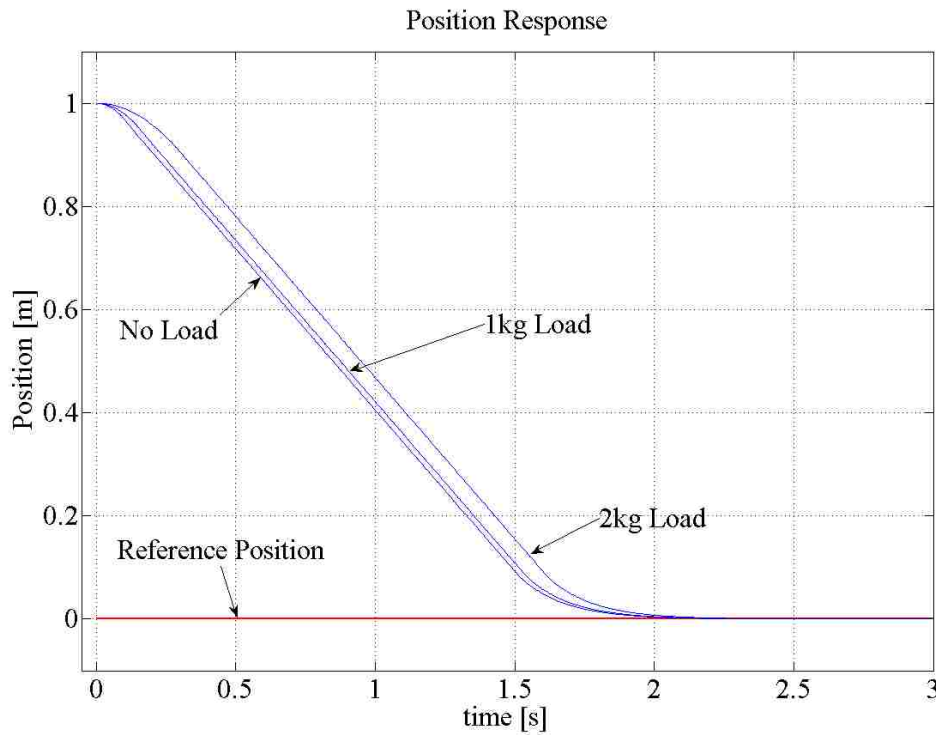


Figure 5.21 Simulated position response of elevator electric drive for descending car carrying no load, 1kg load, and 2kg load

From Fig. 5.20 and Fig. 5.21 it is observed that the addition of a load extends the time during which the motor must accelerate the system from a stand-still, but once in motion the elevator car moves at the maximum allowed speed regardless of what it carries. It is also seen that the car with a load decelerates in less time than the car without a load. It is evident from the data listed in Table 5.1 that placing a load in the elevator car does increase the time it takes for the system to respond to a step change in desired height. It is also shown that the additional time needed is proportional to increased load that added to the car.

Table 5.1 Simulated position response of electric elevator drive with no load and 1kg, 2kg load

	Response Time when Moving Upwards from 0 meters [s]		Response Time when Moving Downwards from 1 meters [s]	
	0.5 meters	1.0 meters	0.5 meters	0.0 meters
To Height:				
Load = 0 kg	0.848	2.712	0.847	2.598
Load = 1 kg	0.882	2.745	0.873	2.625
Load = 2 kg	0.980	2.843	0.950	2.699

Table 5.2 gives the additional time needed for each load as a percentage of the response time for the car without a load.

Table 5.2 Percent change in simulated position response of electric elevator drive under load

To Height:	Up		Down	
	0.5 meters	1 meter	0.5 meters	0 meters
No Load	0.0%	0.0%	0.0%	0.0%
1kg Load	4.0%	1.2%	3.1%	1%
2kg Load	15.6%	4.8%	12.2%	3.9%

Based upon the information contained in Table 5.2, the elevator electric drive and digital control system are able to compensate for loads which are placed in the elevator car and that the variations in response time induced by loads are reduced over greater distances of travel.

5.2 Performance of Experimental Electric Elevator Drive with Position Control

With the simulated performance of the elevator’s electric drive’s position control recorded, the lab experiment is conducted using an elevator model built by the author (see Fig. 5.22). The physical model differs from the simulation model in that the physical model possesses two safety cut-off switches in the event that the elevator car or counter-weight exceeds its range of travel. These safety switches are mounted on the bottom of the elevator’s cover and are connected to an analog-to-digital converter on the dSpace 1104 hardware. A close-up of the safety switch is shown in Fig. 5.23

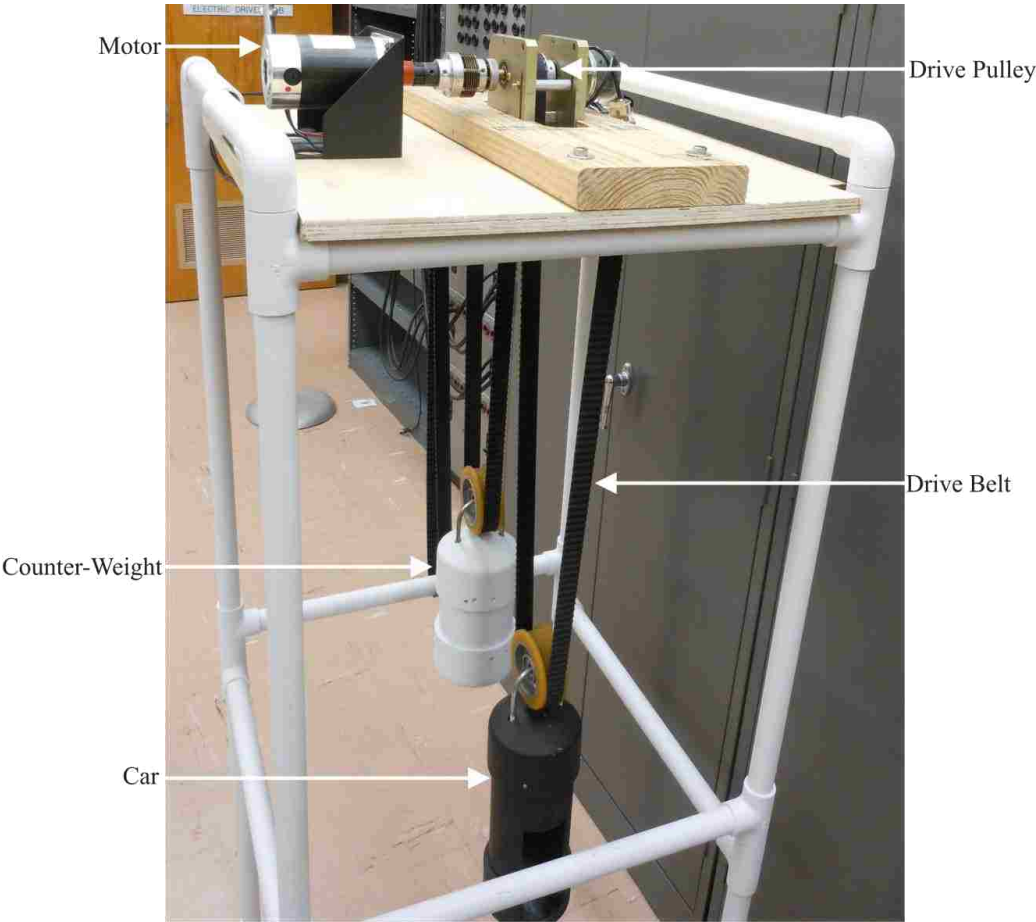


Figure 5.22 View of experimental elevator in lab

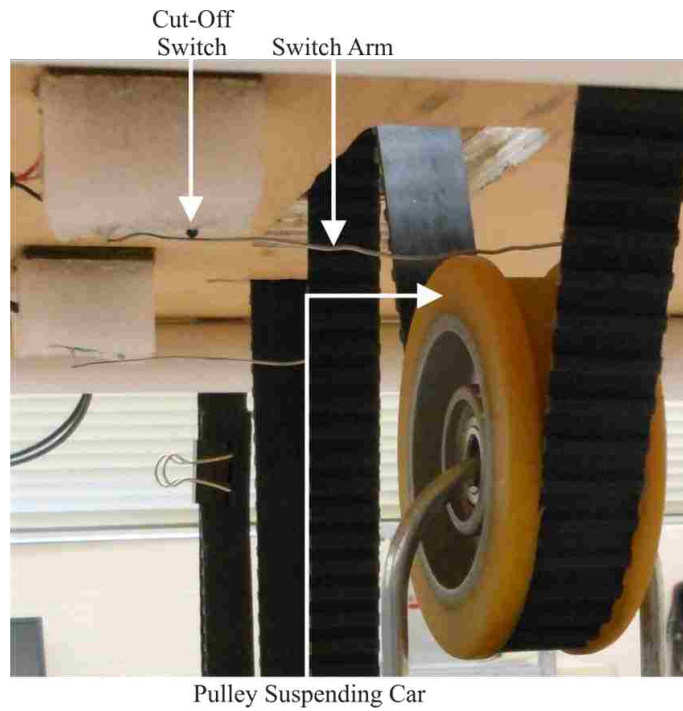


Figure 5.23 Safety cut-off switch

The permanent-magnet DC motor which serves as the elevator electric drive is shown in Fig. 5.24 and is attached to the drive pulley with the drive belt looped over the pulley.

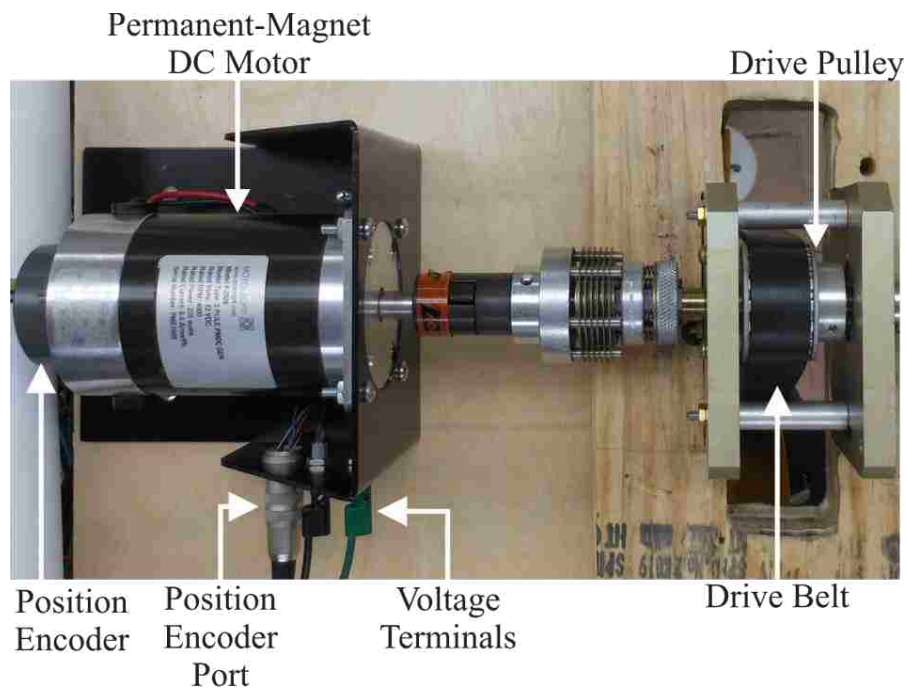


Figure 5.24 View of elevator electric drive and drive pulley with drive belt

Fig. 5.25 shows the PPU which provides power to the permanent-magnet DC motor and Fig. 5.26 shows the dSpace 1104 hardware which contains the analog-to-digital converters, position encoder input, and micro-processor which executes the compiled code [1].

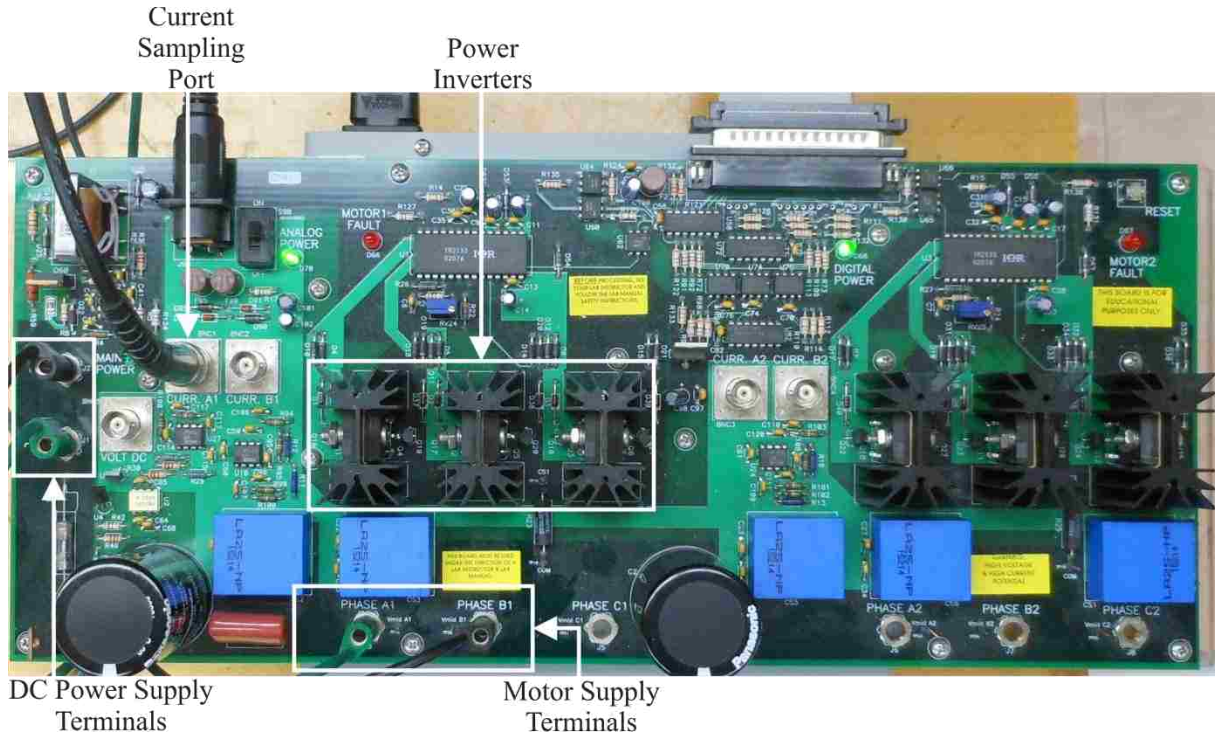


Figure 5.25 Elevator electric drive's power processing unit

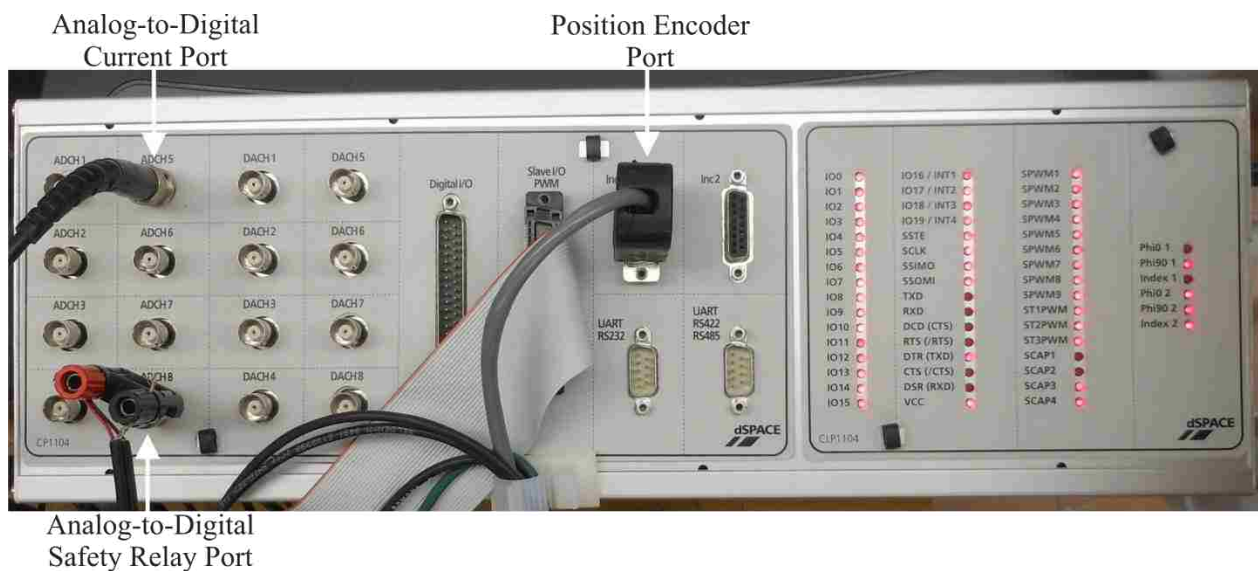


Figure 5.26 dSpace 1104 hardware

The real-time cascaded control system which is compiled and loaded onto the dSpace 1104 hardware is shown in Fig. 5.26. The value of the current as measured by the analog-to-digital converter is passed to the current controller by the ADC block; the motor's speed as measured by motor's position encoder is fed into the control system by the position encoder block. The three control loops shown in Figs 5.27 through 5.29 each have a saturation block which accounts for system limits; the duty ratio generated by the current controller is limited to 1, the reference current generated by the speed controller is limited to the maximum value of current which the power supply can produce, and the reference speed generated by the position controller is limited to the maximum speed with which the elevator can safely operate. The integration block shown in Figs. 5.26, 5.27 and 5.28 can be reset to return the system to its initial conditions. Fig. 5.31 shows the duty cycle generation subsystem which creates two duty cycles from one. These two duty cycles are used to drive the pulse width modulation block which directs the PPU's output.

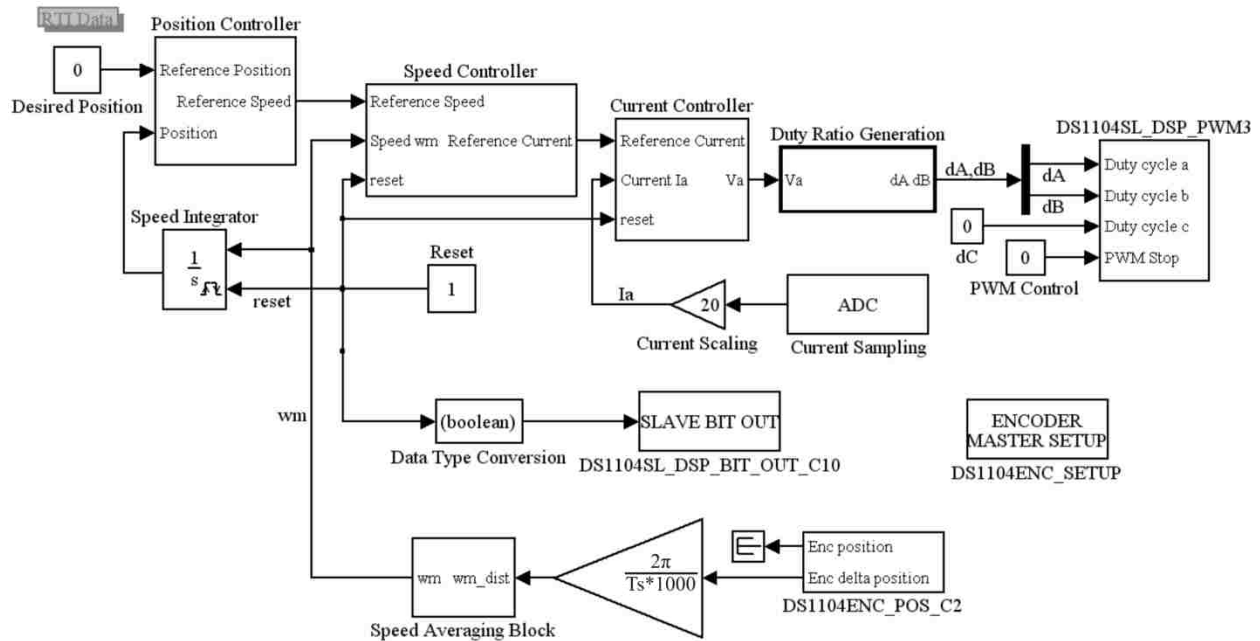


Figure 5.27 Real-time Simulink model for position control of elevator electric drive

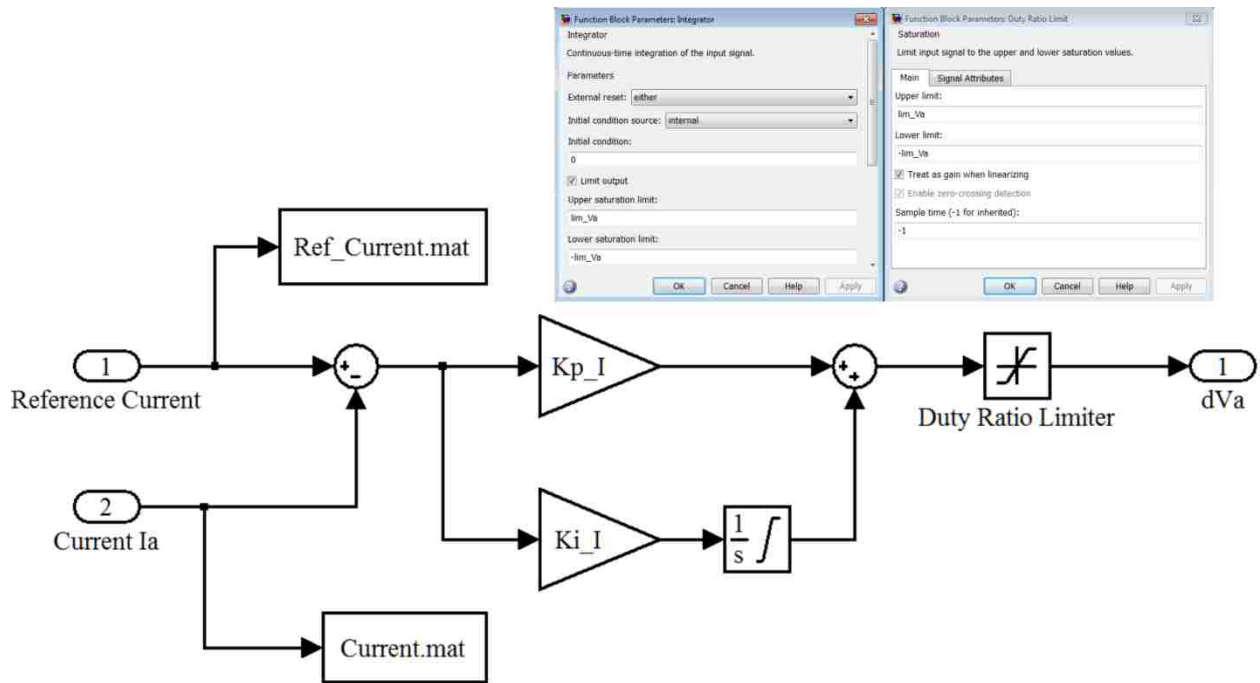


Figure 5.28 Real-time current controller subsystem

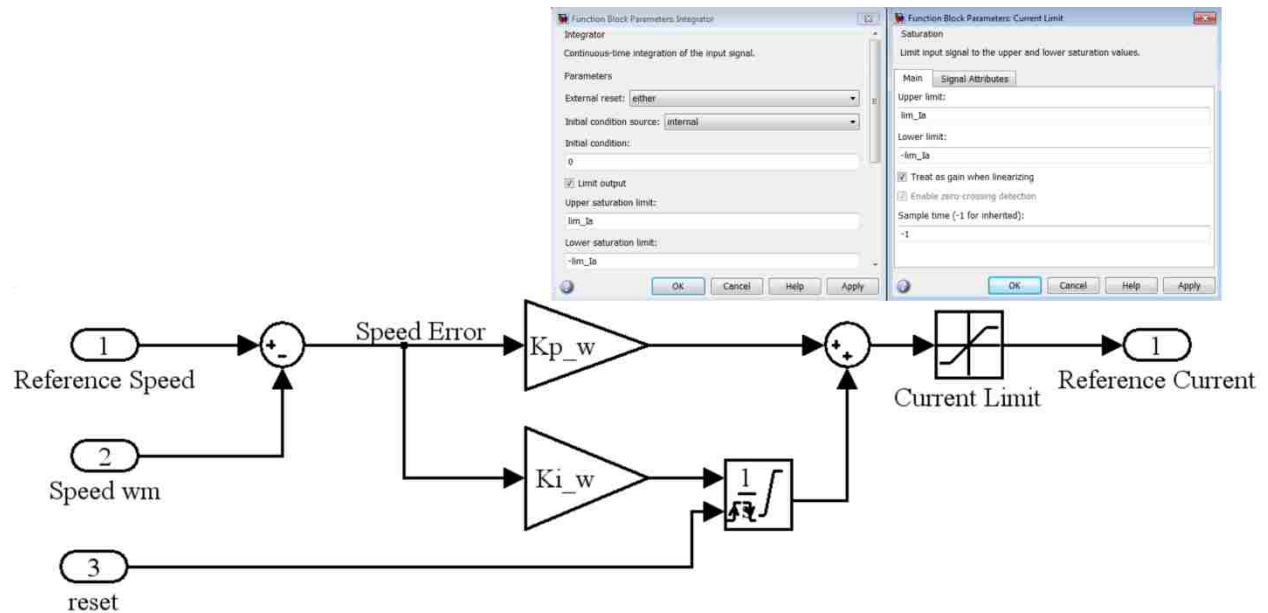


Figure 5.29 Real-time speed controller subsystem

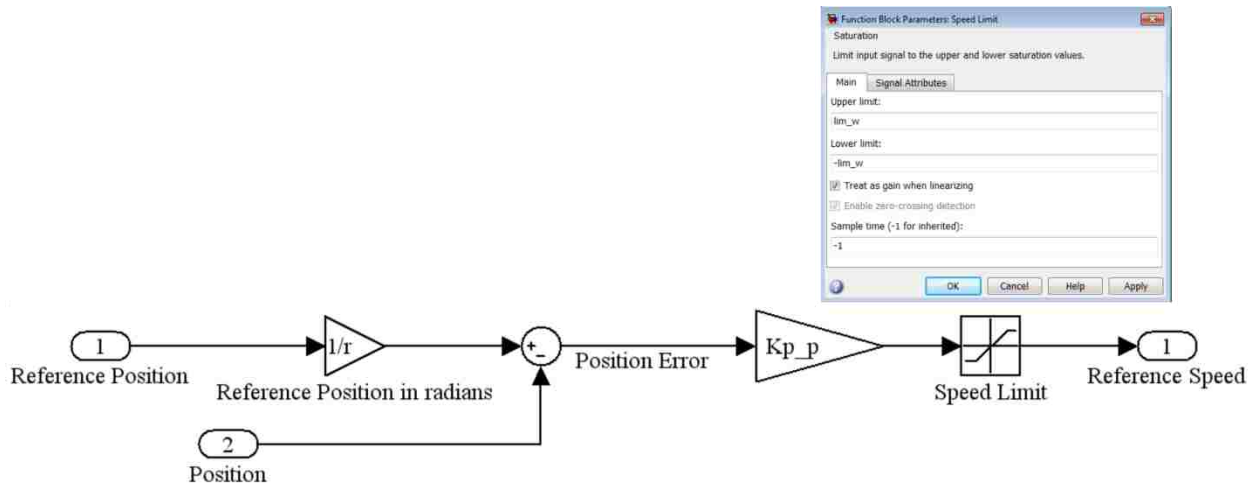


Figure 5.30 Real-time position controller subsystem

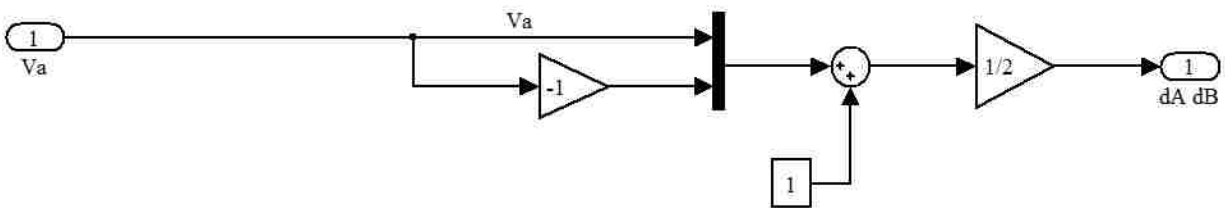


Figure 5.31 Real-time duty cycle generation subsystem

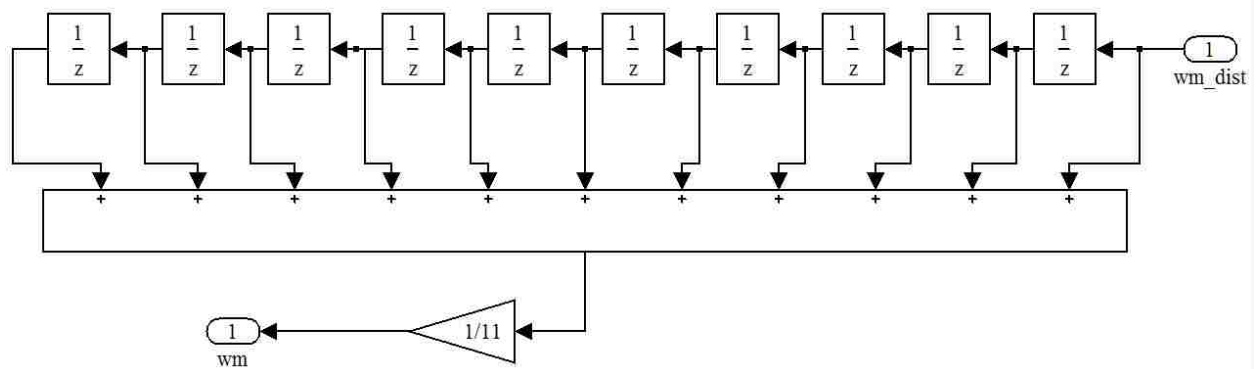


Figure 5.32 Real-time speed averaging subsystem

Before compiling the real-time model, the simulation parameters must be correctly set according to the values shown in Table 5.3.

Table 5.3 Real-time simulation parameters

Start Time	Stop Time	Solver Options	Fixed Step Size	Mode
0.0	Inf	Fixed Step ode1	0.0001	Auto

The Control Desk screen which is shown in Fig. 5.32 is used to input the desired position and to observe the performance of the elevator's electric drive. The instructions on creating the control desk interface and utilizing the interface are contained with the Variable Speed Drives course lab manual [2].

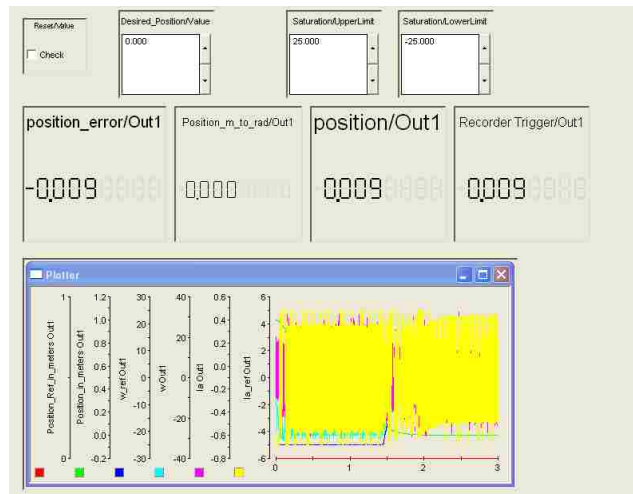


Figure 5.33 Control desk control interface for position control of elevator's electric drive

With the digital control system compiled and loaded into the dSpace 1104's microprocessor, the elevator car loaded with 1kg is directed via the Control Desk screen to ascend 1 meter while data is recorded. After the elevator's car comes to a rest at a height of 1 meter, it is directed to return to the original height of 0 meters while data is again recorded. From the measurements made during these test the performance of the elevator's electric drive can be visually displayed. Fig. 5.33 and Fig. 5.44 show the elevator car's movement upon receiving a change in desired position. The speed at which the motor operates while the car is in motion is shown in Fig. 5.35 and Fig. 5.36 while the current through the motor is shown in Fig. 5.37 and Fig. 5.38.

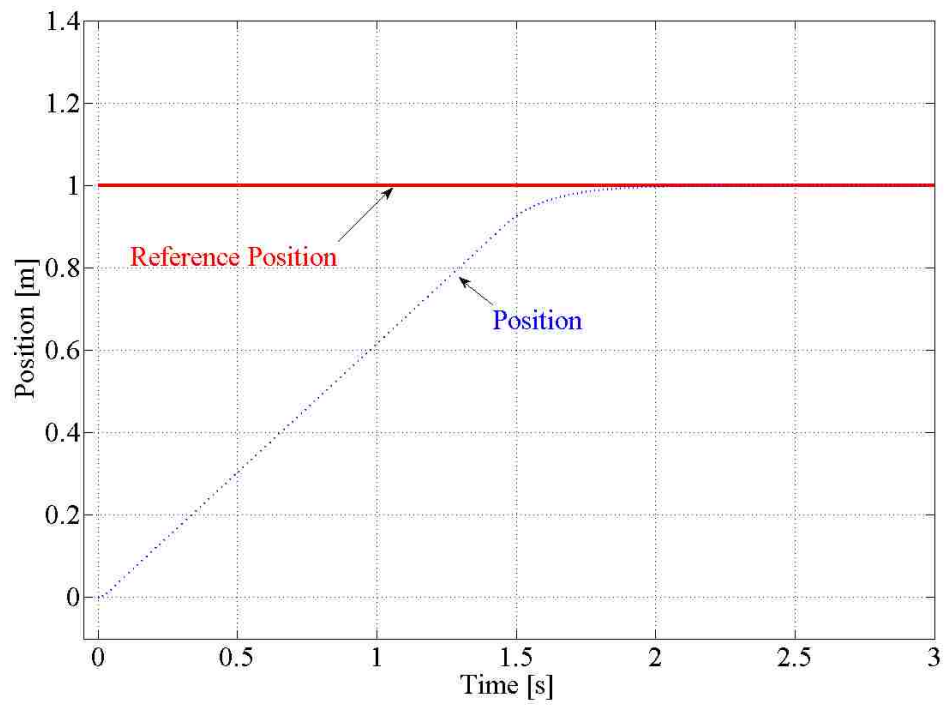


Figure 5.34 Real-time position response of elevator electric drive with ascending car

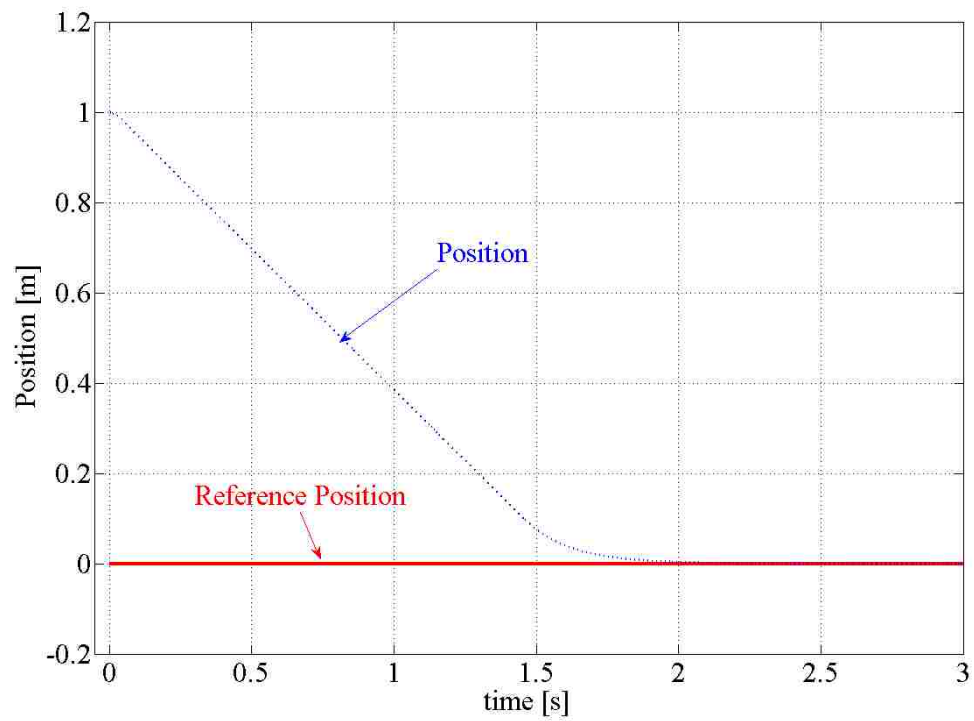


Figure 5.35 Real-time position response of elevator electric drive with descending car

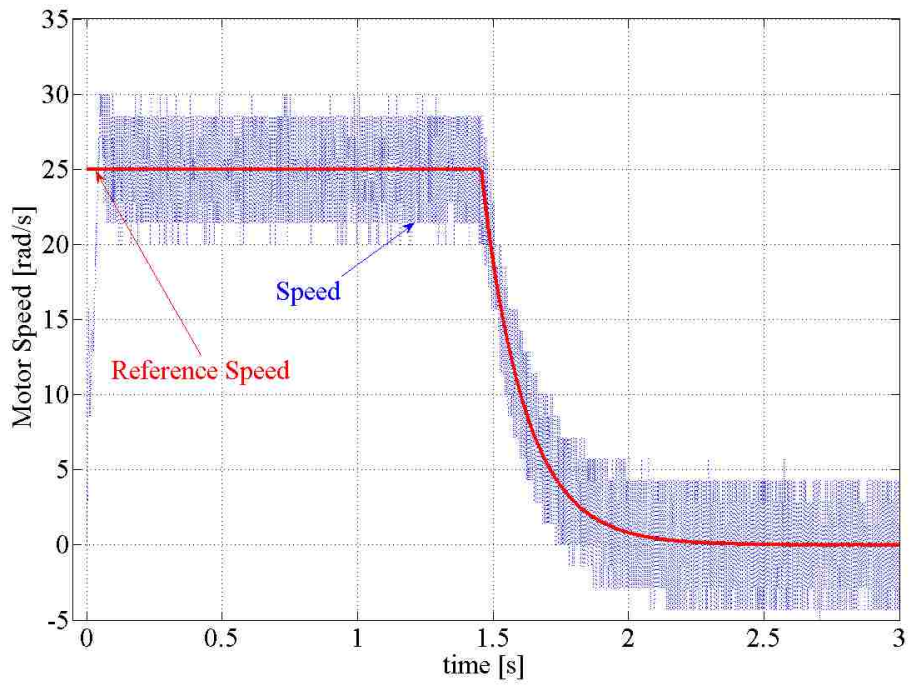


Figure 5.36 Real-time speed response of elevator electric drive with ascending car

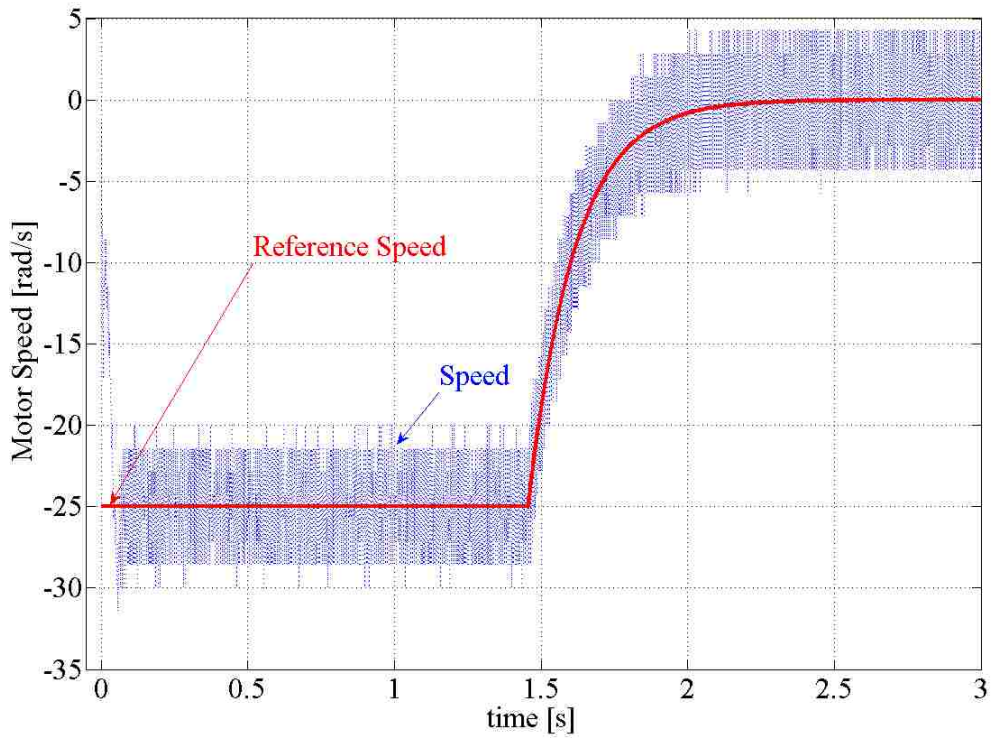


Figure 5.37 Real-time speed response of elevator electric drive with descending car

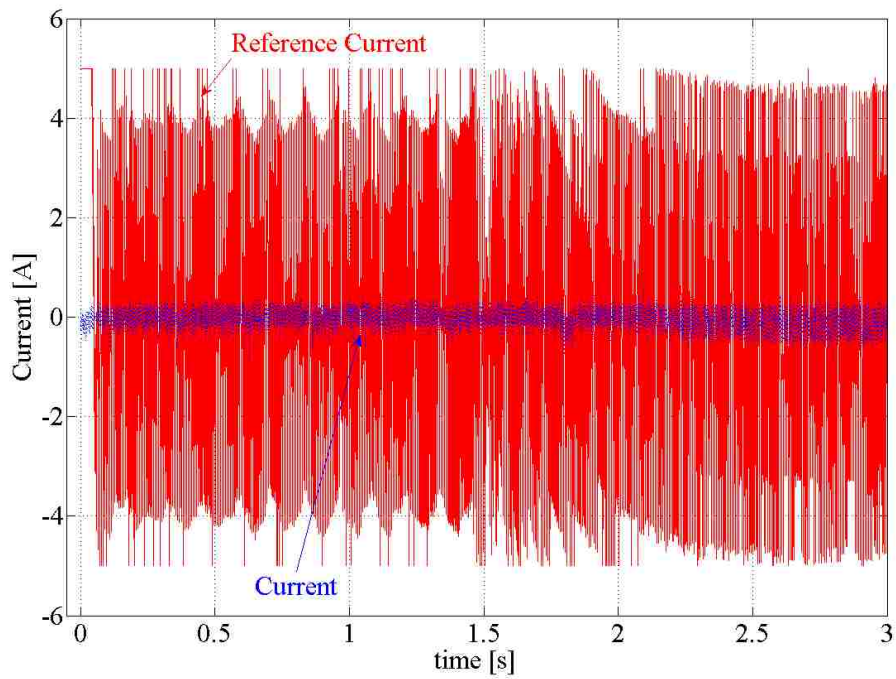


Figure 5.38 Real-time current response of elevator electric drive with ascending car

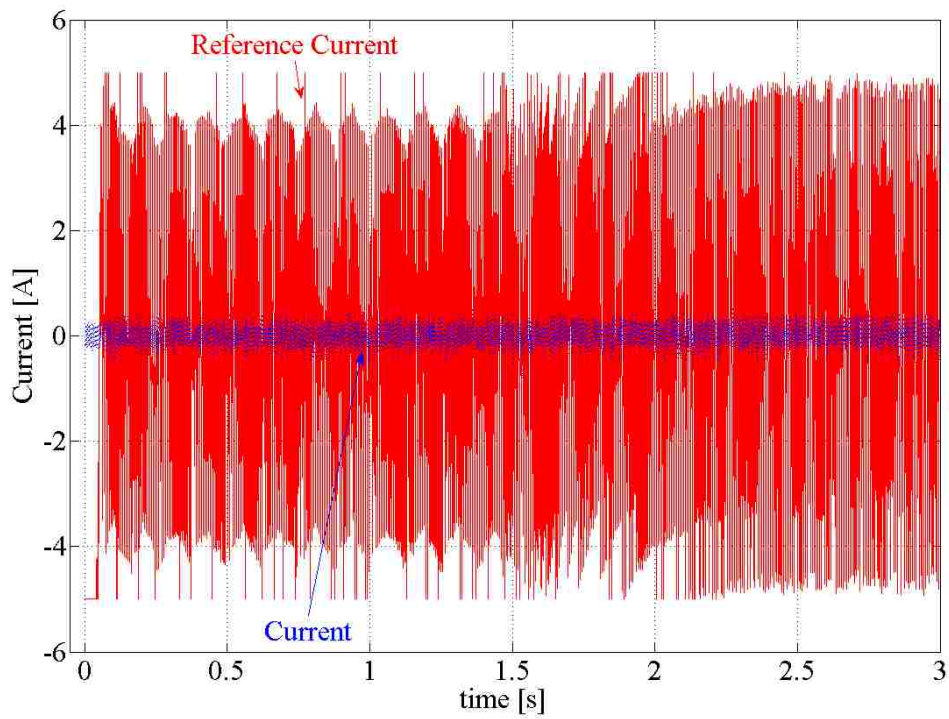


Figure 5.39 Real-time current response of elevator electric drive with descending car

Testing with the experimental elevator electric drive with position control shows that the elevator car can be moved to a desired set point in a smooth and accurate fashion (see Fig. 5.34 and Fig. 5.35).

When moving upwards or downwards, the car accelerates rapidly to the steady-state limit of $25\frac{rad}{s}$ and remains at this speed until the speed controller begins exponentially reducing the reference speed (see Fig. 5.35 and Fig. 5.36). The actual speed never reaches a steady-state error of less than 10% which induces rapid changes in the reference current as shown in Fig 5.38 and 5.39. The actual current drawn by the motor does change with the reference current but the armature winding's inductance dampens the magnitude of change.

The elevator's electric drive system is tested with three variations in load weight, moving both upwards and downwards. The position response of the system for these three variations in load are plotted in Fig. 5.20 for the elevator car moving upwards and in Fig. 5.21 for the elevator car moving downwards.

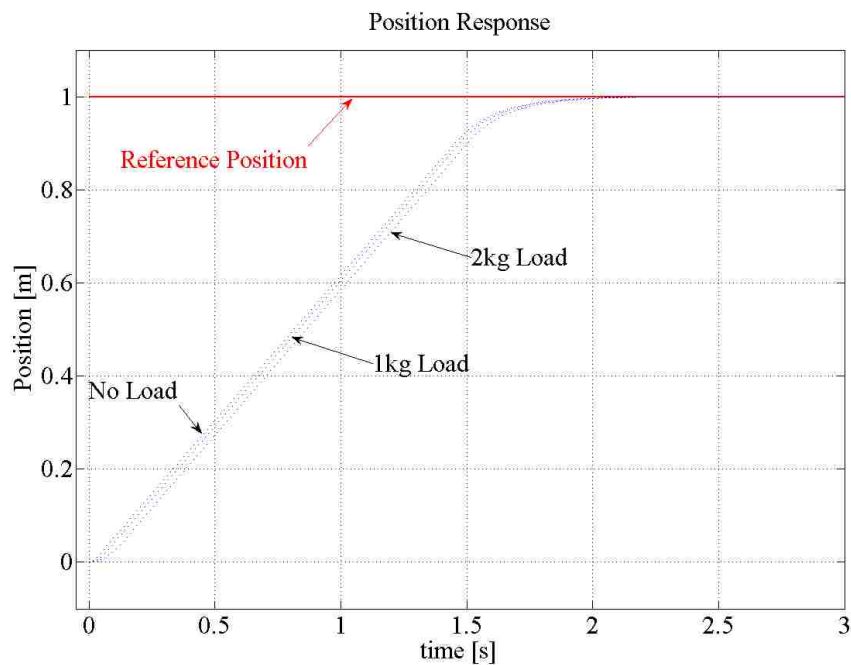


Figure 5.40 Real-time position response of elevator electric drive for ascending car carrying no load, 1kg load, and 2kg load

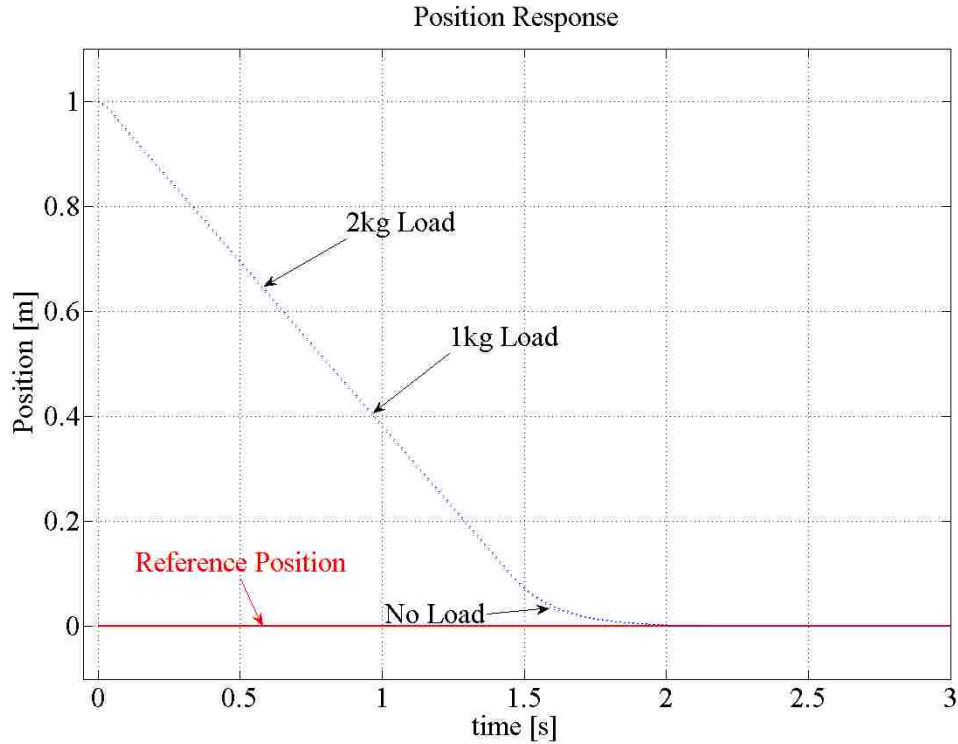


Figure 5.41 Real-time position response of elevator electric drive for descending car carrying no load, 1kg load, and 2kg load

The real-time results of the elevator electric drive show that the addition of a payload to the elevator car has greater affect on the ascending motion than on the descending motion. Despite the increase in inertia when moving upwards, the loaded car does not greatly affect the position response when ascending and descending.

Table 5.3 Real-time position response of elevator electric drive with no load and 1kg, 2kg load

	Response Time when Moving Upwards from 0 meters [s]		Response Time when Moving Downwards from 1 meters [s]	
	0.5 meters	1.0 meters	0.5 meters	0.0 meters
To Height:				
Load = 0 kg	0.815	2.654	0.807	2.600
Load = 1 kg	0.834	2.661	0.813	2.609
Load = 2 kg	0.865	2.670	0.814	2.618

Table 5.4 Percent change in real-time position response of electric elevator drive under load

	Up		Down	
	0.5 meters	1 meter	0.5 meters	0 meters
No Load	0.0%	0.0%	0.0%	0.0%
1kg Load	2.3%	0.3%	7.4%	0.3%
2kg Load	6.1%	6.0%	8.7%	3.9%

5.3 Comments on Performance of Electric Elevator Drive with Position Control

The elevator electric drive with position control has been implemented successfully first as a computer simulation and then experimentally in the lab. The cumulative results of the two procedures are listed in Table 5.5.

Table 5.5 Performance of Elevator Electric Drive

Elevator Car Load	Response Time when Moving Upwards [s]		Response Time when Moving Downwards [s]	
	Simulation	Experimental	Simulation	Experimental
0 Kg	2.712	2.654	2.598	2.600
1 Kg	2.745	2.661	2.625	2.609
2 Kg	2.843	2.670	2.699	2.618

The experimental performance of the electric elevator drive closely followed that of the simulated electric elevator drive. In computer simulation, the speed and current loops both had minimal overshoot with a quick settling time while the position control loop had no overshoot and arrived at the desired value as fast as the speed limiter would allow. During experimental testing, the position control loop had no overshoot and arrived at the desired height as fast as the speed limiter would allow; however, the speed and current control loops never reached steady-state variables due to inaccurate readings from the motor's position encoder. Despite hardware issues, the experimental electric elevator drive was able to meet the desired set-point in less time than predicted by computer simulations.

Chapter 6: Conclusions

The implementation of position control of an elevator's electric drive was analyzed in this thesis. Forces involved in the mechanical system were determined allowing for the calculation of torque generated by the motor and torque placed on the motor by the load. The electric circuit parameters and mechanical system parameters of the permanent-magnet DC motor were empirically derived using a series of measurements collected from experimental test conducted in the laboratory. Using these parameters the current, speed, and position control loops were designed for the elevator's electric drive. The cascaded control system and permanent-magnet DC motor were modeled in Matlab's Simulink package and position control of the elevator's electric drive was simulated for no load conditions and loaded conditions. With the simulated performance of the elevator's electric drive's ability to arrive at a desired position recorded, testing was conducted in the lab using the permanent-magnet DC motor and scale elevator constructed by the author to collect data on the elevator electric drive to arrive at the desired height in a timely and accurate manner. Using data collected from the simulations and testing, the conclusions from this analysis of position control of an elevator's electric drive are:

- It is necessary to determine the electrical and mechanical parameters of an electric motor in order to correctly design control loops which direct the electric motor to the desired position.
- The design of cascaded control loops which direct the electric drive to the desired position must consider the parameters of the drive and the system which it is driving; the individual loops of the cascaded control system must also be coordinated so as to not conflict with one another.

- The computer simulation of the system is an approximation of the actual system and provides an expedient method by which the performance of the system can be predicted. Verifying simulation results with data collected from real-time experiments validates the model and theory on which it is built allowing for rapid development of new applications.

Applying the techniques found within this thesis, a student is able to design and implement digitally controlled electric drives for an unlimited number of applications. The chapter covering the determination of motor parameters is not inclusive of all types of electric drives and the chapter on designing a digital control system does not compensate for all variables a dynamic system may encounter but it does provide a blueprint for upgrading systems which may have older drives and new control systems or for replacing an existing mechanical with an electrical one. Performing the steps of determining motor parameters, designing cascaded control systems, and collecting data in the lab provides a tangible learning experience for students enrolled in LSU's Electrical Engineering course on electric drives.

References

- [1] dSPACE. *DS1104 R&D Controller Board Hardware Installation and Configuration*. User's Manual, March 2004
- [2] Gunda, Kiran K. "Adjustable Speed Drives Laboratory Based on dSPACE Controller". MS Thesis. Louisiana State University, Baton Rouge, May 2008
- [3] Hakala, Harri. "Integration of Motor and Hoisting Machine Changes the Elevator Business". *International Conference on Electrical Machines*, Espoo, 2000, pp.1241-1243
- [4] KONE. *2012 Architectural Planning Guide*. Brochure, 2011
- [5] Mendrela, Ernest A. Lecture notes on Variable Speed Drives. Louisiana State University, Baton Rouge, December 2009
- [6] Mohan, Ned. *Electric Drives: An Integrative Approach*. Minneapolis, MN: MNPERE, 2003
- [7] Otis. *Gen2*. Brochure, 2011
- [8] Otis. *About Elevators*. Brochure, 2011

Appendix A: Load_Simulation_Parameters

Ra=0.864
La=0.0107
Ke=0.0744
Kt=0.0744
B=0.00004 %Friction coefficient
J=0.000741 %equivalent inertia of entire system
Jp=0.000487 %inertia of drive pulley
r=0.025 %drive pulley radius in meters
g=9.8 %gravitational constant
Mc=1.67 %mass of car
Mew=1.67 %mass of counter-weight

Kpwm=40 %Volts
lim_Ia=5 %Amps
lim_Va=1 %Duty Cycle
lim_w=25 %radians/second

Ki_I=32.3
Kp_I=0.40

Ki_w=78.639
Kp_w=1.084

Kp_p=6.283

Appendix B: Plot_Simulation

```
load Position P; load Ref_Position R_P; load Speed w; load Ref_Speed R_w; load Current Ia;
load Ref_Current R_Ia; load Voltage Va; load Torque Tem;
```

```
clf
figure (1)
plot (R_P,'r','linewidth',2)
hold on
plot (P,'--','linewidth',2),title('Position Control Loop'), xlabel('time [s]'),ylabel('Position [m]')
```

```
figure (2)
plot(R_P,'k','linewidth',2)
hold on
plot (P,':k','linewidth',2)
hold on
plot (R_w,'r','linewidth',2)
hold on
plot (w,'--','linewidth',2),title('Speed Control Loop'), xlabel('time [s]'),ylabel('Motor Speed [rad/s]')
```

```
figure (3)
plot(R_P,'k','linewidth',2)
hold on
plot (P,':k','linewidth',2)
hold on
plot (R_Ia,'r','linewidth',2)
hold on
plot (Ia,'--','linewidth',2),title('Current Control Loop'), xlabel('time [s]'),ylabel('Motor Current [A]')
```

```
figure (4)
plot(R_P,'k','linewidth',2)
hold on
plot (P,':k','linewidth',2)
hold on
plot (Tem,'--','linewidth',2),title('Torque'), xlabel('time [s]'),ylabel('Electro-Magnetic Torque [N*m]')
```

```
figure (5)
plot(R_P,'k','linewidth',2)
hold on
plot (P,':k','linewidth',2)
hold on
plot (Va,'--','linewidth',2),title('Armature Voltage'), xlabel('time [s]'),ylabel('Armature Voltage [V]')
```

Appendix C: Plot_RealTime

```
load Position Pos; load Speed w; load Current Ia;
```

```
t = Pos (1,:);  
r = Pos (2,:);  
a = Pos (3,:);
```

```
figure (1)  
plot (t,r,'linewidth',3)  
hold on  
plot (t,a,,'linewidth',3),grid,title('Position Control Loop'), xlabel('Time [s]'),ylabel('Position [m]')
```

```
figure (2)  
t = w (1,:);  
r = w (2,:);  
a = w (3,:);
```

```
plot (t,r,'r','linewidth',1)  
hold on  
plot (t,a,,'linewidth',2),grid,title('Speed Control Loop'), xlabel('time [s]'),ylabel('Motor Speed [rad/s]')
```

```
figure (3)  
t = Ia (1,:);  
r = Ia (2,:);  
a = Ia (3,:);
```

```
plot (t,r,'r','linewidth',2)  
hold on  
plot (t,a,,'linewidth',2),grid,title('Current Control Loop'), xlabel('Time [s]'),ylabel('Current [A]')
```

Vita

Peter James Ford was born in West Monroe, Louisiana. He completed his Bachelor of Science in Electrical Engineering at Louisiana State University Agricultural and Mechanical College in 2009. In August 2010 Peter returned to LSU to pursue his graduate studies; he is a candidate for the degree of Master of Science in Electrical Engineering for May 2012.